The University of Auckland

Galiev, Sh.U., Galiyev, T. Sh.

‘Elastica’-like waves and particles: from Bernoulli, Euler, Laplace and Faraday to the eruption of the Universe

Auckland

2017

Scientific Editor - Professor Garry Tee (The University of Auckland)

ABSTRACT

An information about ‘elastika’-forms is presented. These forms have been mathematically described by Euler in the middle of the 18th century. Some of these forms correspond to the strongly-nonlinear waves propagating in different media. Examples of wave equations describing elastica-like waves are presented. Special attention is given to the nonlinear Klein-Gordon equation. The exact and approximate solutions to this equation are constructed. These solutions describe some elastica-like travelling waves. They can also describe a formation of strongly-localized wave objects in some resonators. It is stressed that these objects (particles, bubbles) can occur during the origin of the Universe and affect its subsequent evolution.

‘Elastica’-like waves and particles: from Bernoulli, Euler, Laplace and Faraday to the eruption of the Universe

Galiev, Sh.U., Galiyev, T. Sh.

Department of Mechanical Engineering, The University of Auckland,
Private Bag 92019, Auckland 1142, New Zealand: s.galiyev@auckland.ac.nz

Contents

1. Introduction and prologue

1.1. Short introduction

Strong nonlinearity is an important element of Nature. Bernoulli and Euler first showed this. They mathematically described strongly-nonlinear forms of very flexible structures (thin strips of elastic material or very flexible initially straight lines). Much later, it was revealed that some of these forms may be excited because of an impact loading of long structural elements. Obviously an analogue was found between elastica forms and strongly nonlinear wave processes. Indeed, Laplace has shown that one of Euler's elastica forms describes capillary waves on the surface of the liquid. This analogue is developed here using many experimental and theoretical data. At the same time our attention is focused on strongly-nonlinear wave processes. Multivalued solutions of nonlinear wave equations are considered, which qualitatively correspond to certain elastica forms. In particular, simplified mathematical models are presented describing these forms. Using these models we study strongly-nonlinear waves propagating in scalar fields (the nonlinear Klein-Gordon equation).

We show that strongly-nonlinear waves can occur during free oscillations of scalar fields in resonators. These oscillations are accompanied by a radiation of jets and particles of energy. Similar oscillations and waves were observed by on surface of water vertically excited in resonators (the Faraday waves) and on surface of sea boiling during vibrations caused by seaquakes, volcanoes and earthquakes. The resonant wave forms resemble the elastica forms of strips and strings which attracted the attention of many of the brightest minds in the history of mathematics and physics.

1.2. Prologue

Euler's elastica forms. The elastica forms of strips attracted the attention of James Bernoulli, Leonhard Euler, Pierre Laplace, Gustav Kirchhoff, Max Born and others [1-10]. In particular, James Bernoulli posed the precise problem of the elastica in 1691. Euler, building on (and crediting) the work of the Bernoullis, was the first to completely characterize the family of curves known as the elastica (Fig. 1). His treatment was quite definitive, and holds up well even by modern standards (Fig. 2).

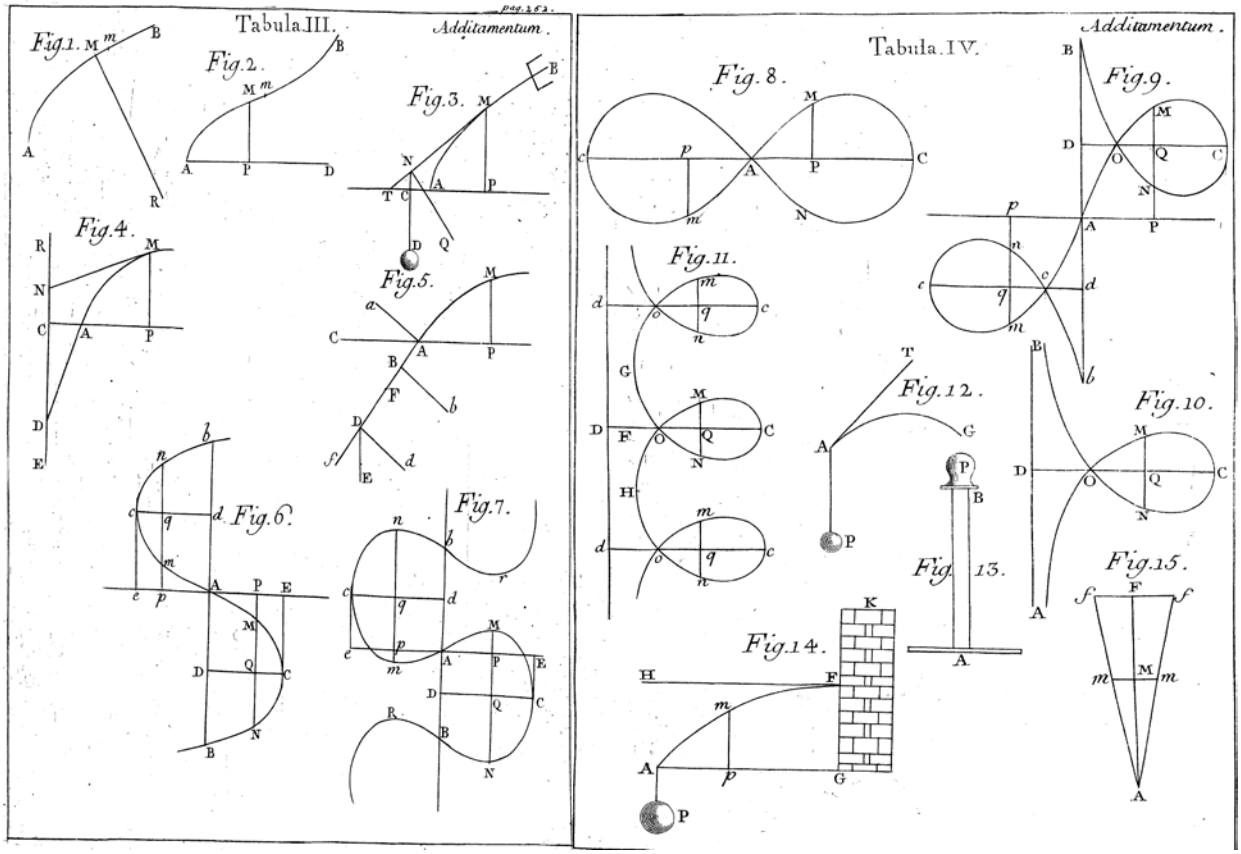

Fig. 1. Six of Euler's elastica figures: Fig.6 –Fig. 11 (left and right) [1].

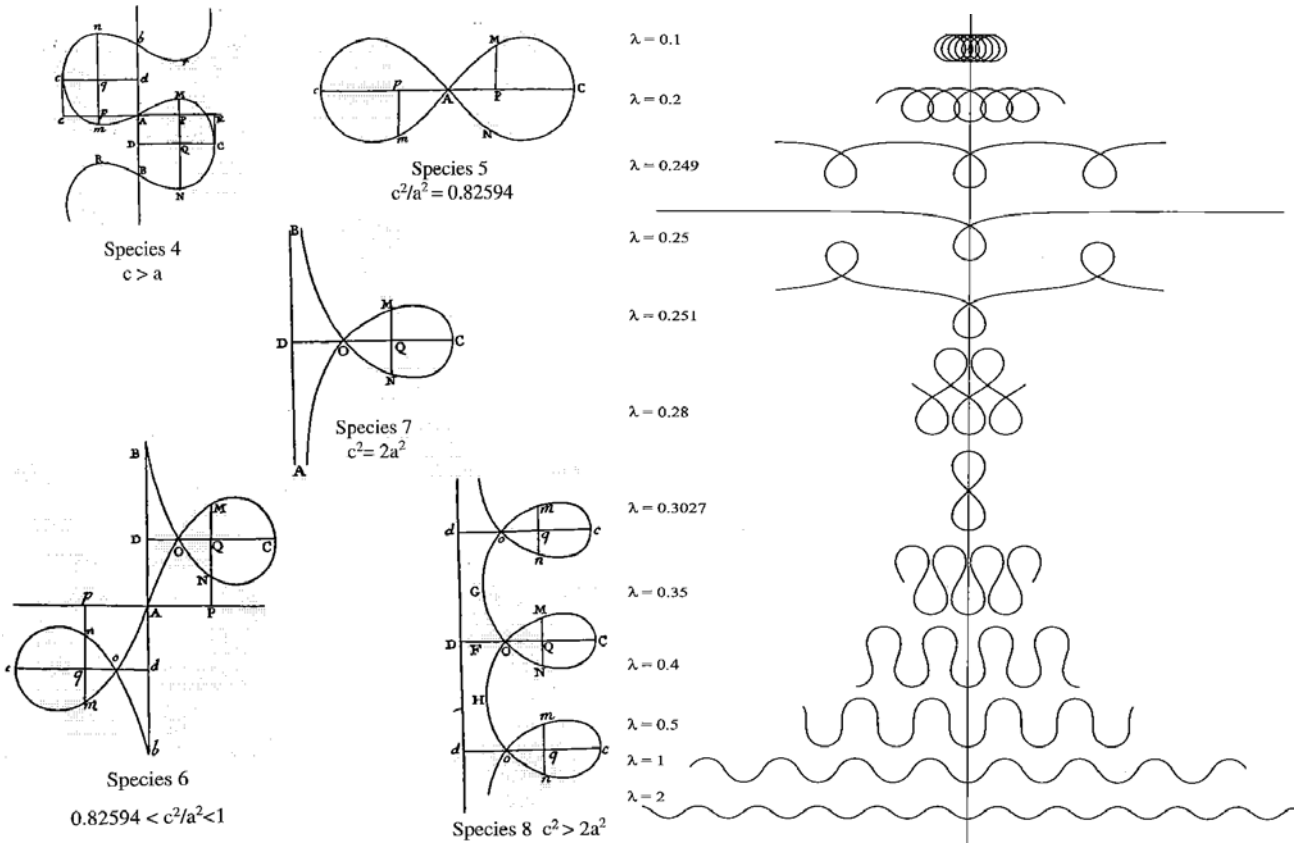

Fig. 2. The evolution of the elastica forms as function of certain parameters *a*, *c* (left) and λ: λ = 0.1; 0.2; 0.249; 0.25; 0.251; 0.28; 0.3027; 0.35; 0.4; 0.5; 1 and 2 (from top to bottom of the picture) (right) [1, 4].

The elastica forms calculated for different values of certain parameters *a* and *b*, and $\lambda = \frac{1}{2}a^2c^{-2}$ are shown in Fig. 2 (see the subsection 1.2.2). The reader can see the transform of the harmonic wave (λ = 2) into the shock-like wave (λ = 0.5) and then into the mushroom-like configurations (λ = 0.4 and 0.35). Euler's elastica (Fig. 1 (left and right) and Fig. 2 (left)) describe well some results of modern calculation showed in Fig. 2 (right). In particular, Euler's elastica 6, 7, 8, 9, 10, 11 (Fig. 1) correspond well to curves $\lambda = 1$, 0.4, 0.3027, 0.251, 0.25 and 0.249 (Fig. 2 (right)).

The folding and formation of relating elastica forms are well-known processes of the instability of many long flexible systems (Fig. 3). In particular, folding and knotting of thin structural elements can take place under an axial impact [11-13].

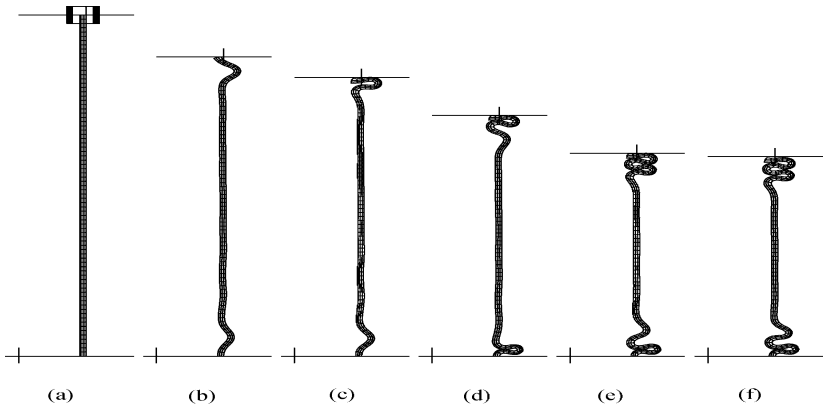

Fig. 3. Development of the dynamic buckling form of a long structure under an impact loading (a) initial, (b) t = 0.322 ms, (c) t = 0.504 ms, (d) t = 0.918 ms, (e) t = 1.598 ms, (f) t = 2.612 ms [12].

The form λ = 0.35 of Fig. 2 corresponds to the tucks arising at axial crushing of the square tube (Fig. 4 left). The shapes presented in Fig. 4 (centre and right) form by the compression of very flexible rods.

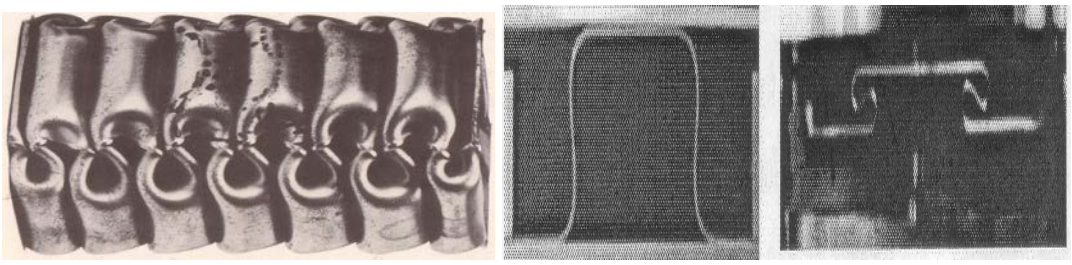

Fig. 4. The folding can take place during the crushing of square tubes left) [11]. Table-like form (centre) and mushroom-like form (right) of a thin rod [13].

Experiments of Sir Taylor and an 'elastica'. Let us consider results of the interesting experiments performed by Sir G.I. Taylor (Fig. 5) [14].

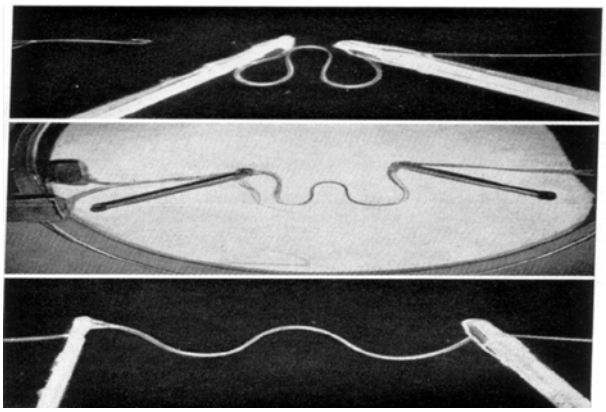

Fig. 5. Threads of SAIB, floating on mercury [14].

Taylor wrote in 1969: "The analogy between the equations of motion of a viscous fluid and that of an incompressible elastic solid is well-known. It was pointed out to me by Brooke Benjamin that when a thin rod is subjected to end compression it forms an elastica and that Love's *Theory of Elasticity* contains a picture of the set of elasticas. I, therefore, found a very viscous fluid, known as SAIB (Sucrose Acetate Isobutirate) and stretched a thread of it between two sticks. I then laid this thread on the surface of a dish of mercury and either pushed the sticks towards one another or laid two matches on the thread and pushed them towards one another, and photographed the thread" (see Fig. 2: λ = 1, 0.5 and 0.4). Sir G. I. Taylor observed also a very viscous stream of the fluid falling onto a plate [14]. A short distance above the plate the stream begins to wave or rotate into a spiral form. More complex folding was observed when the stream falls into a fluid of less density than itself. In the last case the stream can fold and form knots. The folding of the stream resembles the buckling of the elastic bodies which have been showed in Figs. 3 and 4.

Laplace's capillary waves. Apparently, the elastica forms can exist in many highly-nonlinear wave systems. We suppose that the elastica forms can describe qualitatively periodic appearance of splashes, drops and bubbles on a liquid surface as results of highly-nonlinear effects and the surface tension. In particular, the forms which intended for the description of different forms of rods may be used for the analysis of highly-nonlinear capillary waves.

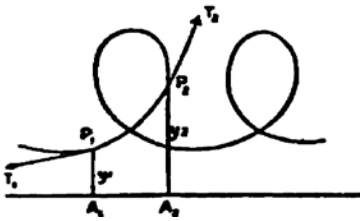

Fig. 6. Some elastica forms can describe the water surface forms which can appears because of the capillarity [1, 7].

Pierre Simon Laplace investigated the shape of the capillary in his 1807 work [7]. We think that the elastica-like waves and their dynamics describe processes which have been observed in many experiments. In particular, parametrically (vertically) forced surface waves, which may be known as Faraday waves [15, 16], can describe as elastica forms [17-19].

Perturbations, the elastica forms (mushroom-like waves) and vortices The evolution of the perturbations of an interface between two environments into vortices was studied in [20]. Fig. 7 was taken from [20]. There theoretical studies of the nonequilibrium Ising-Bloch bifurcation have utilized the FitzHugh-Nagumo reaction-diffusion model and a variant of the complex Ginzburg-Landau equation that describes amplitude modulations of forced oscillations. We can consider the perturbations of the interface as a heterogeneities in the very early Universe.

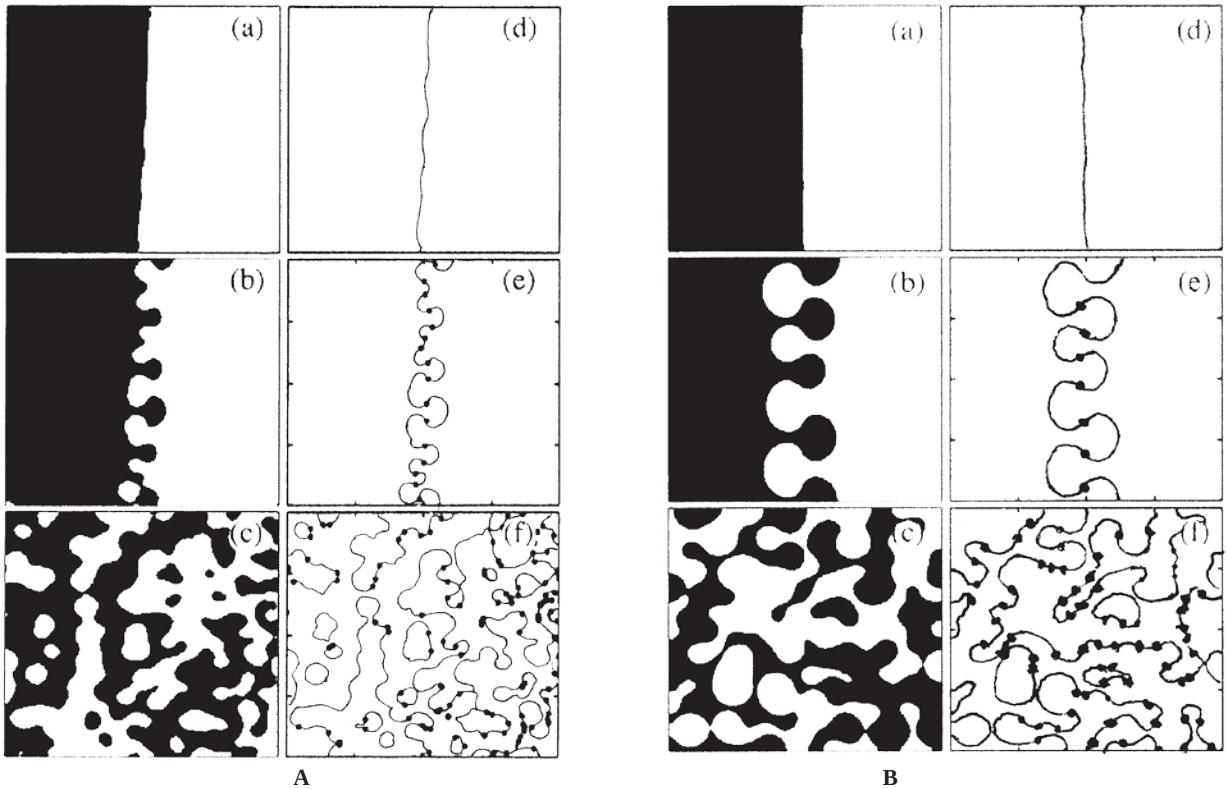

Fig. 7. Evolution of the initial perturbations of some interface into the elasica forms (mushroom-like waves), vortices and turbulence. The occurrence of the vortices shown by spots during the Belousov - Zhabotinsky reaction (**A**). The occurrence of the vortices and turbulence according to the numerical solution of the Ginzburg-Landau equation (**B**) [20]. The formations (e) and (b) resemble that shown in Fig. 1 (Fig. 7) .

The initial interface (a, d) changes as a result of growth of the perturbations. Fig. 7 (e, f) shows the positions of vortices (the spots in the figure) at the different moments of time. Thus, Fig. 7 (d, e, f) demonstrates the evolution of the originally very smooth heterogeneity into elastica-like waves and vortices.

It is possible to give a different interpretation of the presented in Figs. 1-7 results. We have given above the most simple interpretation of the elastica forms (Fig. 1). It is stressed that the strongly-nonlinear forms showed in Figs. 1-7 have much more the big area of applicability, than only the description of a strong bend of long structures and the surface waves. However, we will focus below on the strongly-nonlinear waves.

1.2.1. Nonlinearity: elastica-forms, surface and inner waves

Strongly-nonlinear evolution of waves. Wave nonlinearity is an important element of Nature. In particular, Nature often manifests multivalued solutions (for example, breaking waves and turbulence). Indeed, nonlinear systems often exhibit two or more dynamic equilibrium states for the same values of parameters. For example, internal multivalued oceanic waves can exist for a long time. Their stability is explained by an influence of the environment surrounding a wave. Fig. 8 shows an appearance of similar waves in the liquid flowing in the channel. The originally smooth profile is transformed into the mushroom-like form. The process of the formation of these waves resembles that shown in Fig. 2 (right; $\lambda = 1$, 0.4 and 0.35). Then the last is supplemented by the curls. Further, the flow loses stability and transforms into turbulent.

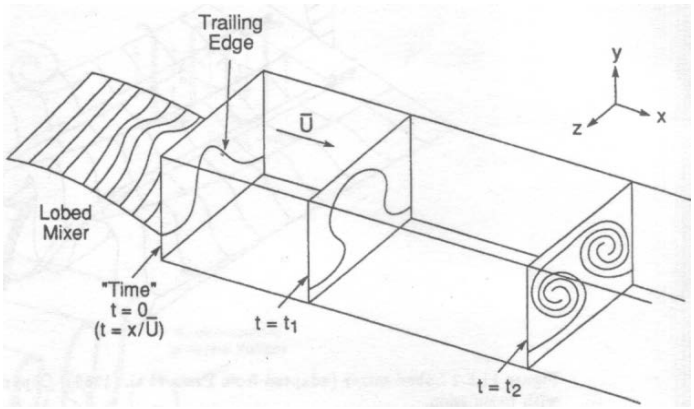

Fig. 8. Evolution of internal waves in the fluid flowing through the channel [21].

Vertical seaquakes can form giant internal ocean waves which resemble presented in Fig. 8. These waves may also appear on the interface of cold and warm ocean water. An example of the appearance and dynamics of similar waves is shown in Fig. 9 [22]. The process of the formation of these waves resembles that shown in Fig. 2 (right; $\lambda = 1$, 0.4 and 0.35). The experiments were conducted using a 3 m drop tower. A

Plexiglas tank containing two liquids with different densities was mounted on a linear rail system, constraining its main motion to the vertical direction. The instability of the interface is generated by dropping the sled onto a coil spring, producing a nearly impulsive upward acceleration. The subsequent free-fall that occurs as the container travels upward and then downward on the rail allows the instability to evolve in the absence of gravity. The interface initially has a well-defined sinusoidal perturbation that quickly inverts and then grows in amplitude, after undergoing the impulsive acceleration.

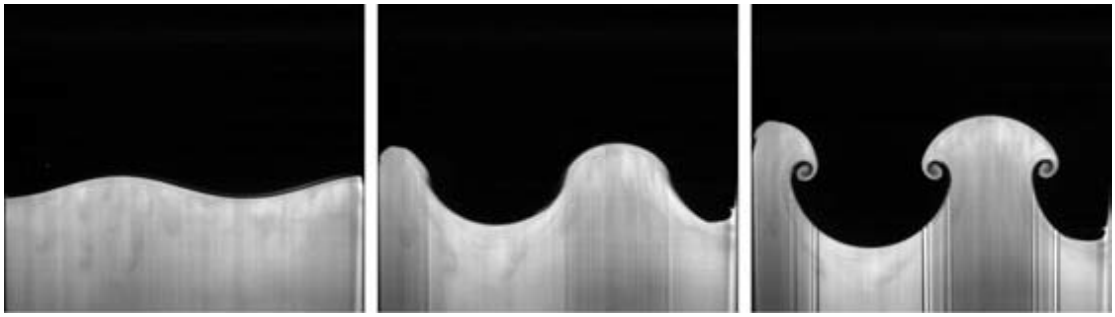

Fig. 9. An example of strongly-nonlinear standing waves appearing on the interface of two liquids with different densities. This a sequence of waves is generated due to the Richtmyer–Meshkov instability of incompressible liquids. The interface has initially the low-frequency sinusoidal perturbation [22]. The waves resemble some forms showed in Fig. 2 (right; $\lambda = 1$, 0.4 and 0.35).

Fig. 9 gives some information about the internal waves rising during earthquakes and seaquakes. However, the complex seaquake phenomena on the free surface of water are not quite clear; but it appears that these phenomena resemble the Faraday effect (vertically –induced parametric resonance) [15, 16].

Resonance is a classical problem of great practical import. This phenomenon is usually associated with oscillations of a point-like mass. For example, the vertical motion of any upper layer may be analysed using the model of a ball. However, some experiments and observations showed that the such a model cannot describe the complex phenomena within the layer and on its boundaries [18, 19]. Sometimes wave properties must be taken into account.

The surface atomization. Of course, multivalued waves, such as those in Figs. 8 and 9, are possible in the most various environments and fields, wherever there is enough strong interaction of media together with the manifestation of strongly-nonlinear effects [18, 19]. In certain cases the surface tension is responsible for appearance of such waves. Namely, the behaviour of systems consisting of 2 or more adjoining environments (phases) can be determined by a thin layer of the contact between these environments (phases). For example, in the case of very short surface waves the mechanical properties of such surfaces are characterized, first of all, by the surface tension. This tension defines properties of a surface similar to properties of a thread (string).

Vertically-induced nonlinear surface waves may be accompanied by collapsing craters. The specified phenomena were noted by many observers of the sea boiling during vibrations caused by seaquakes, volcanoes and earthquakes.

During the last two decades, some surprising nonlinear wave phenomena have been observed on free surfaces of some vertically excited media. Fig. 10 shows a few video frames of a surface of a water drop (2×2 mm) which was vibrated in the vertical direction in its fundamental axisymmetric mode [23]. The frames demonstrate the evolution of surface crater into surface jet.

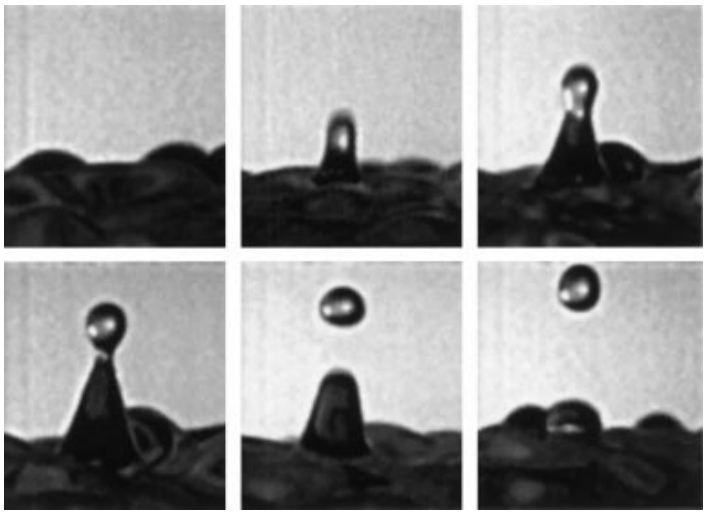

Fig. 10. A time sequence of images of a small part of the drop surface [23].

When droplet ejection begins from the free drop surface (Fig. 10), the wave motion on it appears to be mostly chaotic. During this motion on the free surface a depression, or a crater, precedes the rising liquid spike that ultimately ejects the secondary droplet. This is similar to the spike observed after the collapse of a cavity caused by an air bubble that has just broken through the free surface of a liquid layer from below. Another phenomenon which can be compared with the bursting is the impact of a drop on a solid surface or a liquid layer. In either case a crater is formed, followed by a jet that may eject several secondary droplets. The process of the eruption of a drop out of a wave crest was modelled in [24]. The results of the calculations are presented in Fig. 11.

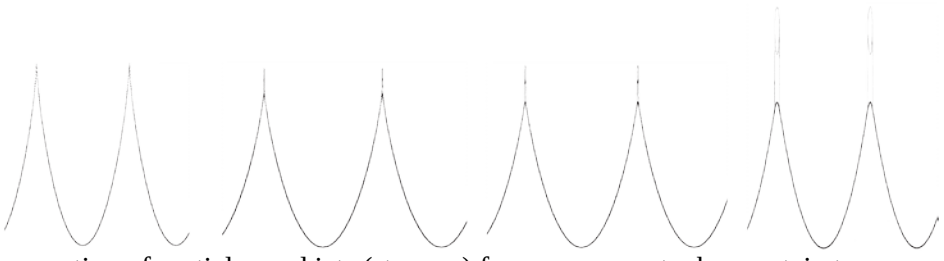

Fig. 11. The eruption of particles and jets (streams) from wave crest when certain transresonant parameter varies from positive to negative values [24].

The process of the formation of the surface crater and the ejected wave (Fig. 10) resembles that shown in Fig. 11.

Surface jets and folds. Vertically-excited counterintuitive waves were observed during experiments described in [25]. The waves presented in Fig. 12a were excited in a vertically-oscillating container, with length of 0.6 m, width of 0.06 m, and depth of water was 0.3 m. The wave crests erupted streams of water, or sometimes they were crowned by small travelling breakers. Fig. 12a demonstrates these waves, which can be schematized as modes A, B and C. Experimental data of Fig. 12a are modelled and illustrated by Fig. 12b and Fig.12c.

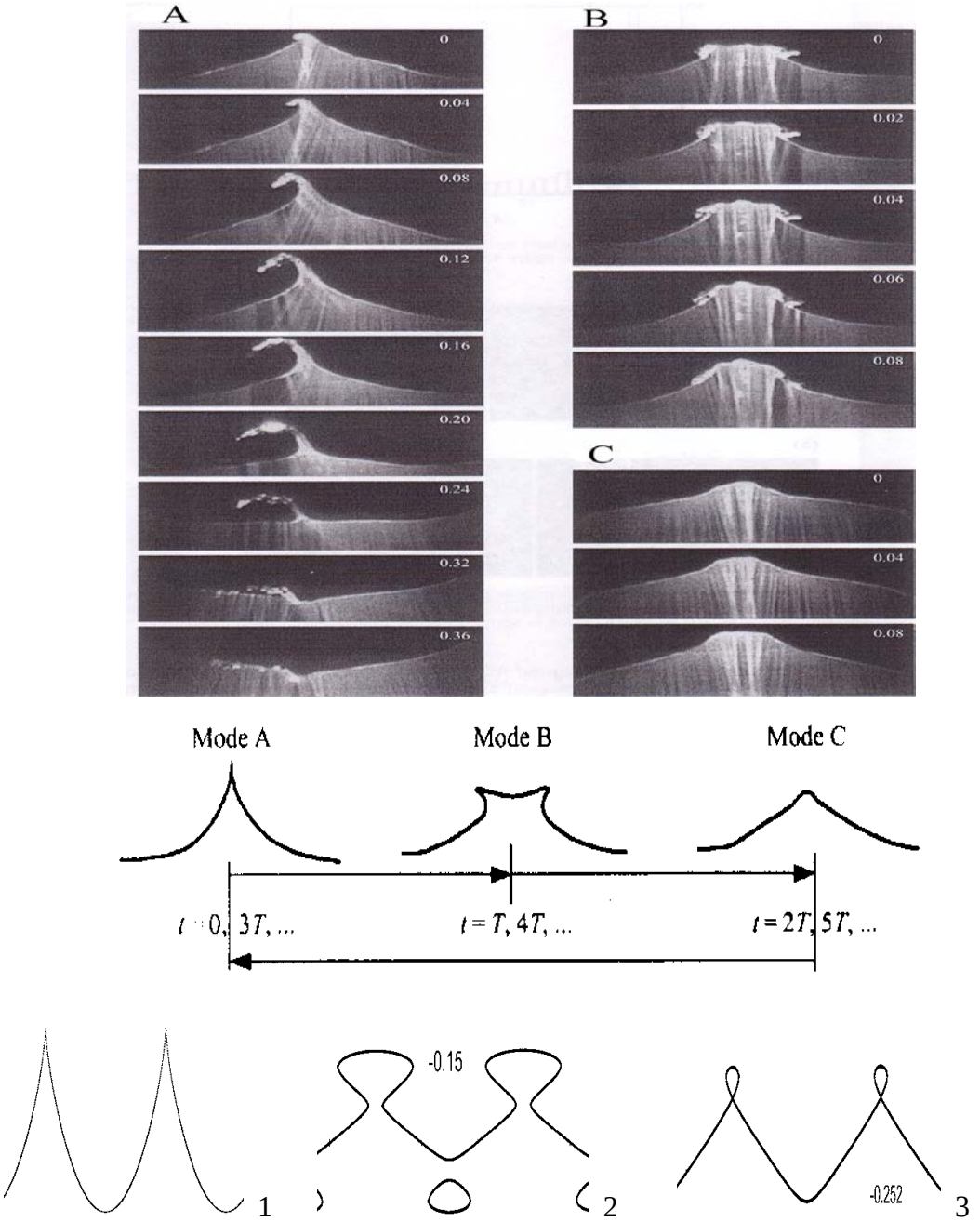

Fig. 12a. Profiles of counterintuitive waves [25, 18, 19]. The modes resemble some forms shown in Figs. 1 and 2.

The mode A in Fig. 12a is defined by a sharp angle at the crest and by the appearance there of a jet. The mode B is characterized by almost-plane or slightly-concave peak, and by the presence of folds on the crest edges. The mode C has a dome-like crest. Counterintuitive profiles of these waves appeared at the container centre.

We emphasize that inside the resonant bands, counterintuitive waves can occur. We found a few curves resembling modes A, B and C – those curves are denoted in Fig. 12a by numbers 1, 2 and 3. The curve (wave) 1 reproduces one of the curves of Fig. 11. The curve (wave) 2 corresponds to the mode B, but this wave is accompanied by the bubble under the wave trough. The curve (wave) 3 corresponds to the mode C.

Results of calculations modelling of experimental data of Fig. 12a presented in Fig.12b [18]. It is seen that curves A, B and C of Fig. 12b qualitatively correspond to photos A, B and C of Fig. 12a.

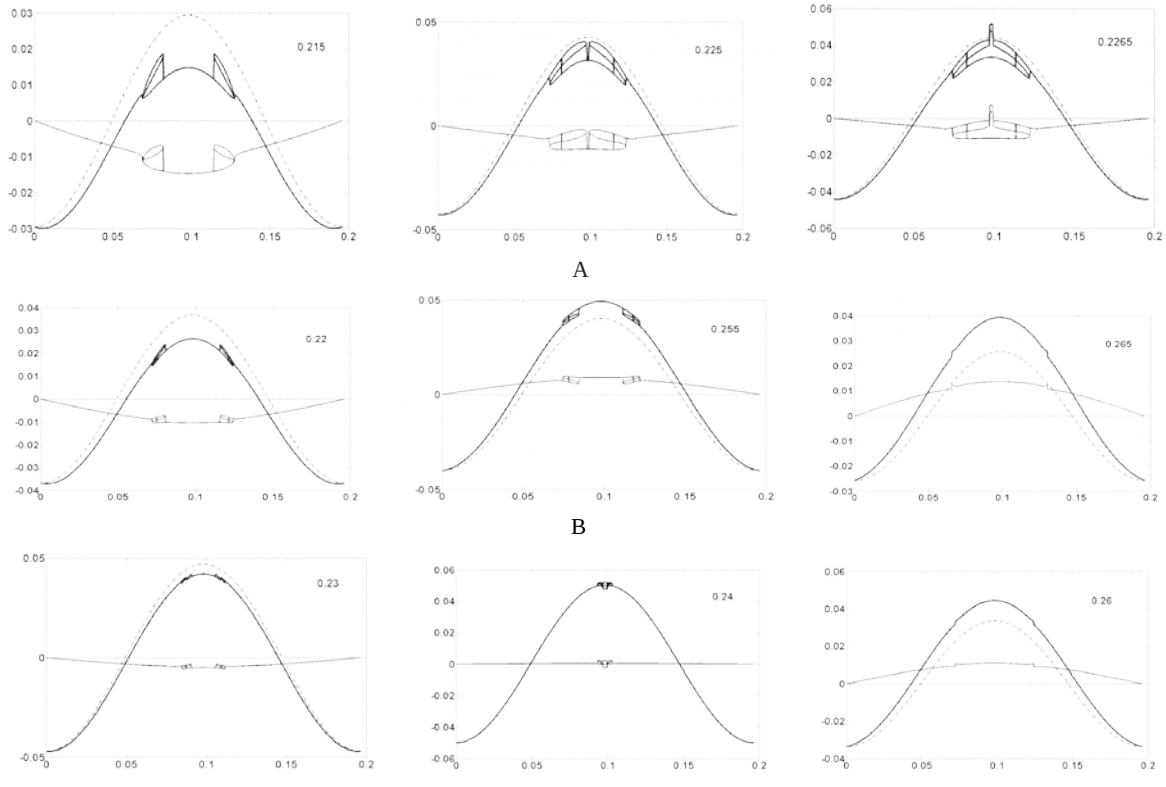

Fig. 12b. The transresonant evolution of waves. The simulation of the vertically excited waves of Fig. 12a. The dash-dot lines determine the initial standing wave. The thin lines determine the elastica-like waves (they are formed by opposite travelling waves). The thick lines are a sum of the dash-dot lines and the thin lines [18].

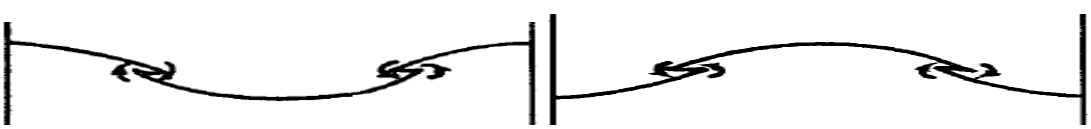

Fig. 12c. The opposite travelling breaking waves which form a structures resembling Euler's Fig 7 (see Fig. 1) [26].

The travelling breaking structures on a interface two liquids forced in a resonator were observed in [26] (Fig. 11c). It is seen that the travelling breaking structures (Fig. 12c left) are qualitatively modelled by the thin lines 0.215, 0. 22, 0.225, 0.23 of Fig. 12b and the travelling breaking structures (Fig. 12c right) are qualitatively modelled by the thin lines 0.255, 0. 26, 0.265 of Fig. 12b.

Strongly-nonlinear Faraday's waves. Michael Faraday [15] began to study the effect of vertical vibrations for a layer of weakly-cohesive materials. He found that small heaps were being formed and a slow convection of the particles took place due to the vibrations. Recent experimental studies of vertically-vibrated granular media and liquids have demonstrated a rich variety of nonlinear wave phenomena. In particular, for acceleration down larger than g, the effective gravity becomes negative and the layer loses contact with the base. The material can exhibit surprisingly complex behaviour. This includes states with the particles forming surface waves, or a 'cloud' with little or no structure. We stress that Fig. 13 illustrates some from noted phenomena.

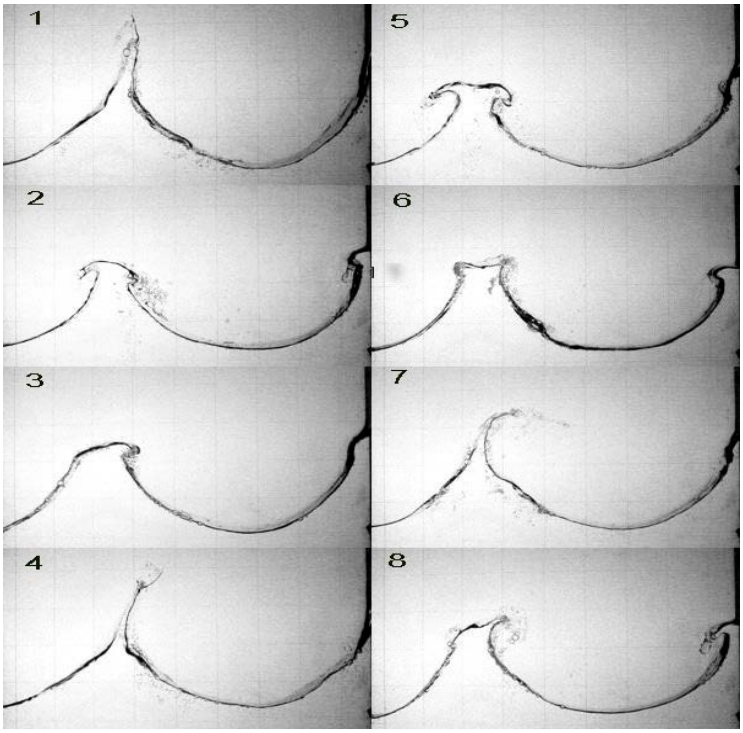

Fig. 13. Destruction of water surface by the Faraday's waves [28].

Results presented in Fig. 12a were amplified in Kolesnichenko's researches [27, 28]. He studied the wave forms excited on water surface by strong vertical vibrations. At the whole, his results presented in Fig. 13 correspond well with data of Fig. 12a. In particular, wave 1, waves 2, 5 and 6, waves 4, 7 of Fig. 13 resembles curve 1, curve 2 and curve 3 of Fig. 12a, correspondingly. On the other hand, the mushroom-like waves 2, 5 and 6 describe qualitatively Fig. 7 of Euler (see Fig. 1).

Conclusion. According to the presented results there are analogue between Figs. 6 and 7 of Euler (Fig.1; see, also, in Fig. 2 $\lambda = 2,1,0.5,0.4$ and 0.5) and the strongly-nonlinear waves (see, for example, Figs. 9 and 13). On the other hand, Figs. 6 and 7 of Euler (Fig.1; see, also, in Fig 2 $\lambda = 0.251,0.25$ and 0.249) describe the formation on the water surface of craters and water drops (Euler's figures 9, 10, 11 and 12 in Fig. 1).

1.2.2. The basic approaches to the study of elastica forms and elastica-like travelling waves

Many problems of physics can be reduced to the solution of nonlinear ordinary differential equations of the form

$$y_{xx} = \overline{F}(y_x, y, x). \tag{1}$$

In particular, this equation describes the elastica forms of different long thin bodies (see Figs. 3-5). On the other hand, it describes unidirectional one-dimensional travelling waves propagate in different media. Let us consider different simplified cases of this equation which have explicit or approximate solutions.

A wide class of the equation (1) can be presented in the form

$$y_{xx} = B + B_1 y + B_2 y^2 + B_3 y^3 + ... + B_n y^n + F(x). \tag{2}$$

Here $F(x)$ is some forced term. Let $F(x)$=0. In this case we can easily find that

$$\tfrac{1}{2} y_x^{\,2} = By + \tfrac{1}{2} B_1 y^2 + \tfrac{1}{3} B_2 y^3 + \tfrac{1}{4} B_3 y^4 + ... + \tfrac{1}{(n+1)} B_n y^{n+1} + C\,. \tag{3}$$

And

$$\frac{dx}{dy} = \frac{1}{\sqrt{2(By + \tfrac{1}{2} B_1 y + \tfrac{1}{3} B_2 y^2 + \tfrac{1}{4} B_3 y^3 + ... + \tfrac{1}{(n+1)} B_n y^{n+1} + C)}}. \tag{4}$$

Here C is a constant of integration. Then we can find that

$$\int dx = \int \frac{dy}{[2(By + \tfrac{1}{2} B_1 y^2 + \tfrac{1}{2} B_2 y^2 + ... + \tfrac{1}{(n+1)} B_n y^{n+1} + C]^{0.5}}. \tag{5}$$

The problem lies in evaluating the integral on the right-hand of (5). For the functions with a highest nonlinearity of y^3, the solution can be expressed in terms of what are known as elliptic functions.

1. Elastica forms. Euler used the following expressions to describe the elastic forms [1, 4]

$$\frac{dx}{dy} = \frac{a^2}{\sqrt{(c^2 - y^2)(2a^2 - c^2 + y^2)}} - \frac{c^2 - y^2}{\sqrt{(c^2 - y^2)(2a^2 - c^2 + y^2)}} \tag{6}$$

and

$$\frac{ds}{dy} = \frac{a^2}{\sqrt{(c^2 - y^2)(2a^2 - c^2 + y^2)}}, \tag{7}$$

where a and c are constants and $s=\sqrt{dx^2+dy^2}$. Solutions of (6) and (7) may be expressed using elliptic functions. Euler classifies the solutions to (6) and (7) using the parameters a and c (Fig. 2 left).

To simplify the analysis of (6) Levien [1] proposes the use of a single λ to replace both a and c:

$$\lambda=\tfrac{1}{2}a^2c^{-2}. \tag{8}$$

Using only λ Levien constructed the forms presented in Fig. 2 (right). We emphasise that all elastica forms obtained by Euler and many strongly-nonlinear travelling waves may be described by the equation (2) [29].

Below we give a few examples of solutions of (2).

1. a. Let $B=0$, $B_2=0$ and $B_n=0$. In this case we can present (2) as

$$y_x^2=A(y^2-y_+^2)(y^2-y_-^2). \tag{9}$$

Here y_+^2 and y_-^2 are roots of the equation $B_3y^4+2B_1y^2+4C=0$. Let (Fig. 14)

$$y=y_+\sin\theta \text{ and } y_x=y_+\theta_x\cos\theta. \tag{10}$$

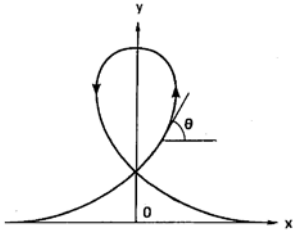

Fig. 14. Elastica form.

In this case the equation (9) may be presented as the following

$$\theta_x^{\,2}+R(\cos\alpha-\cos\theta)=0. \tag{11}$$

Here R and α are constants. The equation (11) is the particular case of the equation

$$\theta_{xx}+\lambda_1\sin\theta+\lambda_2\cos\theta=0. \tag{12}$$

The differential equation (12) expressing curvature as a function of arclength is equivalent of differential equation (6) for the elastica. This equation was derived by Kirchhoff [8]. In particular, he found that 'the state of the rod leads to the same differential equation as the problem of the rotation of a heavy rigid body about a fixed point'. This kinetic analogue is useful for developing intuition about the solutions of the elastica equation. In particular, it is easy to see that all solutions are periodic, and that the family of solutions is characterized by a single parameter [1].

We stress that Love [2] studied many Eular's elastica using the equation (11).

2. Filippov [30] suggested to consider some elastica forms as solitons. Three examples of these solitons were given him in 1986 [30] (Fig. 15)

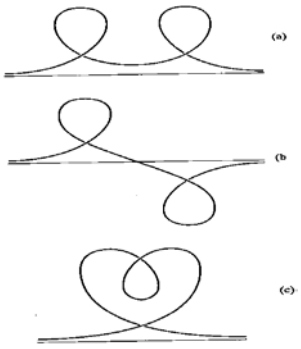

Fig. 15. Examples of Euler's soliton. Two solitons (a), soliton-antisoliton (b), a planar deformation of two soliton configuration (c) [30].

Galiev and Galiyev [29] tried to stress that many wave equations may be simplified to the ordinary differential equation (2). We again emphasize that many types of strongly-nonlinear travelling waves are described by the equation (2). So often their analysis reduces to the calculation of elliptic integrals [1-4, 31-33]. These calculations are not always simple.

2.a. As an example we consider the wave equation [33]

$$u_{xt} = u + \tfrac{1}{6}(u^3)_{xx}\,. \tag{13}$$

In order to seek travelling-wave solution of (13) a new variables were introduced

$$z = \frac{u}{|v|^{1/2}}\ , \quad \eta = \frac{x - vt - x_0}{|v|^{1/2}}, \tag{14}$$

where z is an implicit or explicit function of η, and v and x_0 are arbitrary constants with $v \neq 0$. In this case after some calculations (13) becomes [33]

$$z_\zeta^2 = B^2 - (z^2 + 2c)^2, \tag{15}$$

B is a real positive constant and ζ is defined by

$$\frac{d\eta}{d\zeta} = z^2 + 2c\,. \tag{16}$$

The equation (15) is the particular case of the equation (3). It can be shown that the expression (15) describes the elastica forms presented in Fig. 1 (Figs. 6, 7, 8, 9, 10). Thus, some strongly-nonlinear waves (elastica-like waves) can be described by the elliptic functions. In spite of similar successes, we again repeat that calculations using elliptic integrals are not always simple. Therefore, for the qualitative study of periodic elastica-like waves some artificial method was used in [24, 29]. It was based on the replacement of the second derivative in the equation (2) by a harmonic term.

3. As a result, it was found that certain elastica forms may be described by solutions of strongly-nonlinear algebraic equations [18, 19, 24, 29, 34, 35]. On the other hand, these equations describe wave forms similar some of the elastica forms. Examples of counterintuitive behaviour of these wave forms are presented in Figs. 16 and 17.

Let us consider curves calculated according to the analytical solution of the equation

$$y^3 + (3R / 2^{2/3}) y + \cos \omega a_0^{-1} (a_0 t - x) = 0 \ . \qquad (17)$$

Here R, ω and a_0 are constants. The equation (17) demonstrates the generation (R=0.4), the evolution $R = -0.8$, -0.99999 and bifurcation $R = -1.01$ of the elastic-like waves.

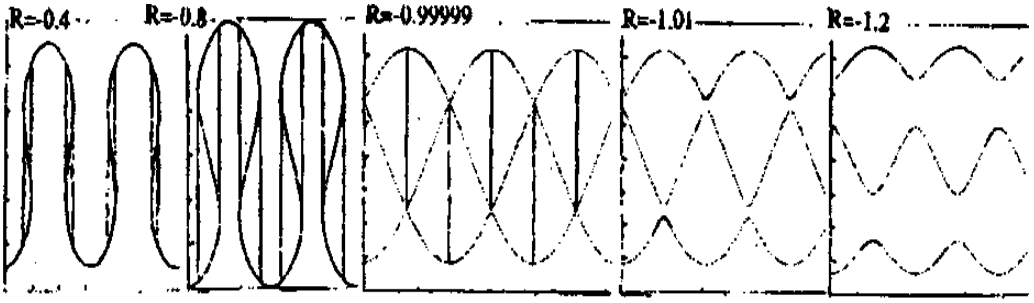

Fig. 16. Displays the generation (R=0.4) and the trans-resonant evolution of the elastic-like travelling wave [29].

The saw-type pyramidal waves may be generated as a result of the bifurcation. Three types of the harmonic waves may be generated in the system according to the analytical solutions outside of the resonant band if $R = -1.2$.

Fig. 17 shows more clear the evolution of elastica-like wave if the parameter R have been changed according to expression $R = 0.03\omega a_0^{-1}(a_0 t - x)$ **[ ].** We assume that R varies from -0.06 to -1.35. One can see smooth evolution of wave into the elastic forms corresponding to $\lambda = 0.5, 0.4$ and 0.35 (Fig. 2).

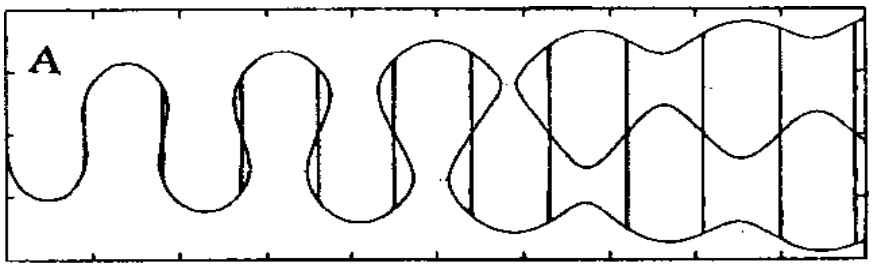

Fig. 17. The evolution of the elastica-like wave [24], when R varies from -0.06 to -1.35.

The wave dynamics of Figs. 16 and 17 resembles the wave evolution shown in Fig. 18.

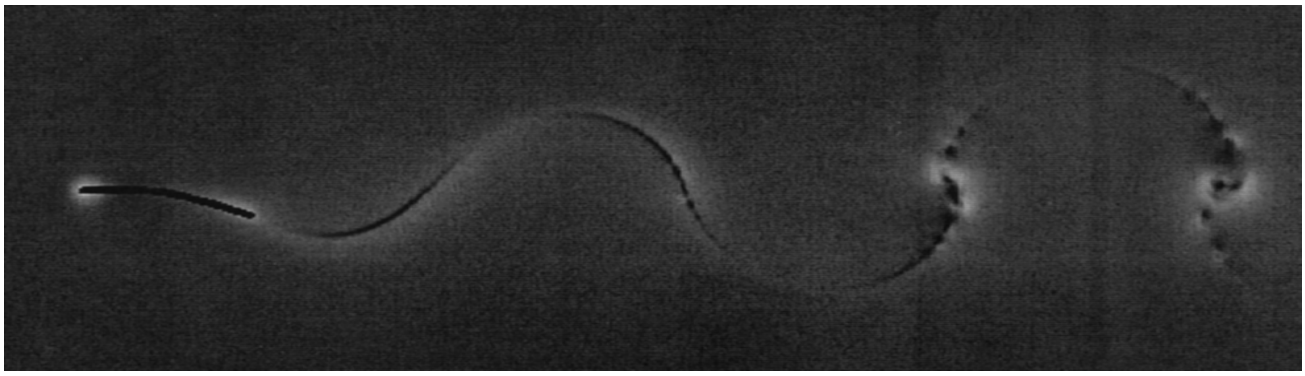

Fig. 18. Photo of Mark Murray and Laurens Howl (Duke University, CNCS) [18].

3.a. The quadratic effect on the elastica-like waves was studied using equation

$$y^3 + r_* y^2 + (3R / 2^{2/3}) y + \cos \omega a_0^{-1} (a_0 t - x) = 0. \tag{18}$$

The wave evolution is studied for different r_* and R (Fig. 19). In Fig. 19 (left) these parameters vary discretely. In Fig. 19 (right) the parameter R varies continuously from −0.3 to −1.4 [24]. At the whole, the results resemble presented in Figs. 16-18. However near $R \approx -1$ the elastic-like waves transform into drop- or bubble-like structures. The drops and the bubbles resemble Euler's figure 11 showed in Fig. 1. The form of the drop-like structures depends on R. These structures transform into of cnoidal-like waves, if R reduces approximately from −0.9 to −1.123. The linear solution (harmonic wave) follows then.

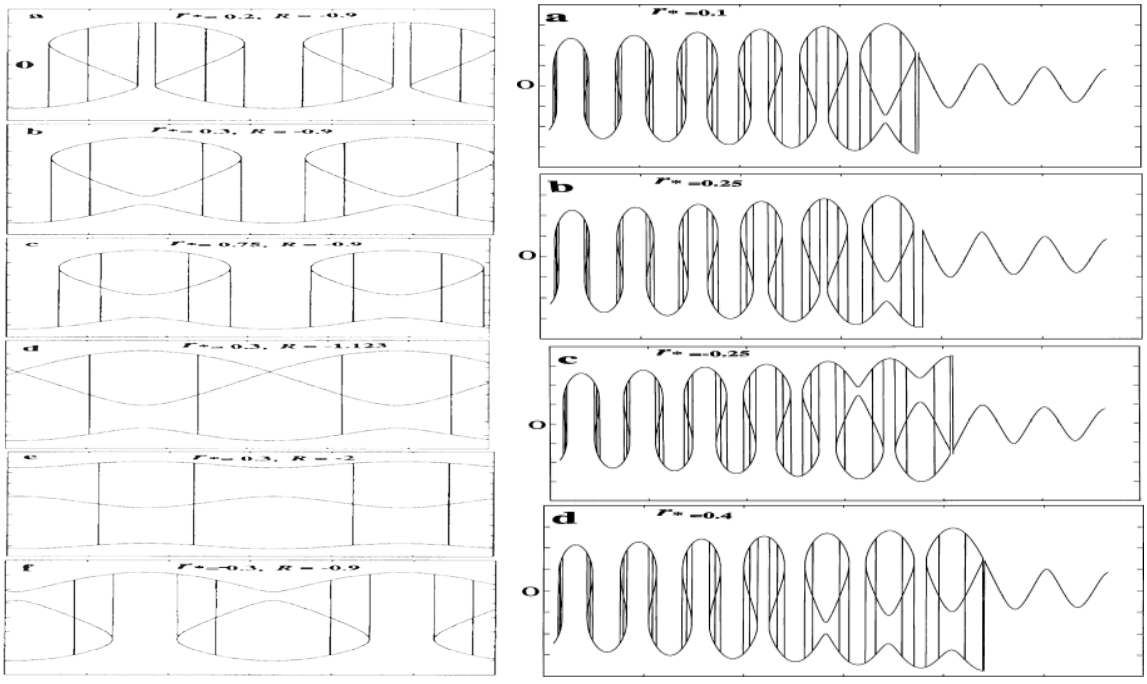

Fig. 19. Quadratic effect. Evolution of the elastic-like (mushroom-like) waves (a) into particles (drops) above the wave crests (b, c) or bubbles below the wave troughs (f) (left). Evolution of the elastic-like (mushroom-like) waves into particles (drops) above the wave crests (a, b, d) or bubbles below the wave troughs (d). R is varied from −0.3 to −1.4 (right).

It is seen that the transresonant evolution of the waves depends upon the quadratic non-linearity. In particular, for r_*= 0.1 we have one drop-like structure, but for r_*= 0.4 four drop-like structures are generated during the transresonant evolution of the ripples (Fig. 19 right). Thus, the elastica-like wave can evolves into drops or bubbles which appear above or below the surface of the wave.

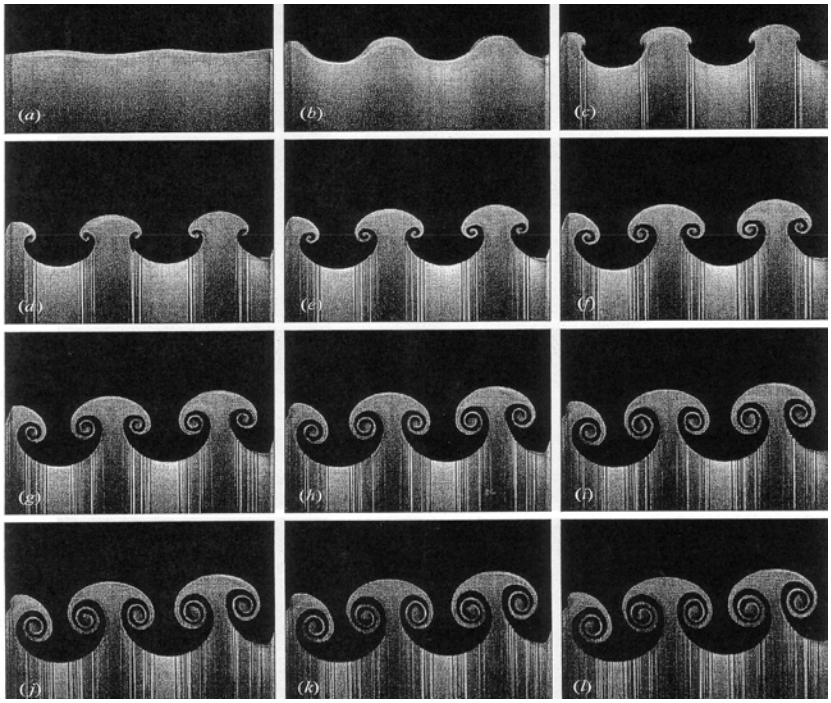

Fig. 20. An example of strongly-nonlinear standing waves appearing on the interface of two liquids with different densities. The interface has the low-frequency sinusoidal perturbation [22]. The waves resemble Figs. 7 and 11 of Euler (Fig. 1).

We can expect that the waves presented in Figs. 16-19 may be formed in different unstable systems during impact actions. Indeed, the wave forms presented in Figs. 16-19 are similar to the wave shapes generated due to the Richtmyer–Meshkov instability of incompressible liquids (Fig. 20, see, also, Fig. 9).

2. Examples of strongly-nonlinear wave equations and solutions of them

Nature is infinitely various in the manifestations. At the same time, if to look at it attentively, Nature does not love 'the pomp of superfluous causes' (Copernicus). This old and deep thought is supported by science data more and more .

The laws of mechanics known as Newton's laws, but actually, presented first by Galilei, Descartes and Newton's other predecessors, showed the common character of huge variety of the mechanical phenomena. This unity would be impossible to imagine earlier. Even more deep and general bases of Nature were opened by Darwin's evolution theory, atomic model of substance and idea of genes. According to this progress, probably, the theory of Everything, which will integrate and explain all main physical phenomena, may be formulated in future.

This theory should be nonlinear.

2.1. Unidirectional waves

1. Many long waves may be described by the strongly-nonlinear equation [18, 19, 29],

$$u_{tt} = c_0^2 u_{aa} (1 + u_a)^{-\gamma - 1}. \tag{19}$$

Here u is a displacement, a is a Lagrangian coordinate, t is time, $u_a = \partial u / \partial a$, $u_t = \partial u / \partial t$ and c_0 is the wave speed. γ is a constant. The equation (19) describes one-dimensional waves in solid bodies, gas, liquids and gassy materials. Taking into account the quadratic and cubic nonlinear terms, we can write the equation (19) for surface waves

$$u_{tt} - c_0^2 u_{aa} = \beta u_a u_{aa} + \beta_1 u_a^2 u_{aa} + k u_{aatt} . \tag{20}$$

Here $\beta = -(\gamma + 1) c_0^2$ and $\beta_1 = 0.5(\gamma + 1)(\gamma + 2) c_0^2$, $k = \frac{1}{3} h^2 - \sigma \rho^{-1} g^{-1}$. For water γ =2. We introduced in (20) a small phenomenological term which take into account the effects of the dispersion ($\frac{1}{3} h^2$) and the surface tension (capillarity) ($\sigma \rho^{-1} g^{-1}$). The last term may be very important for waves propagating in thin layers.

The common solution of equations similar (20) is not known. However, the particular solution of the equation (20) can be received in the assumption that

$$u = u(r), \;\; r = a - ct . \tag{21}$$

Here c is the wave speed. In this case the equation (20) is transformed into the ordinary differential equation which has the first integral

$$B(u_r)_{rr} = B_3 (B_1 B_3^{-1} u_r + B_2 B_3^{-1} u_r^2 + u_r^3 + C_1 B_3^{-1}) \;\; . \tag{22}$$

Here B, B_1, B_2 and B_3 are the constants and C_1 is a constant of integration. Now new unknown value Φ is introduced:

$$\Phi = u_r + \tfrac{1}{3} B_2 B_3^{-1} \ . \tag{23}$$

In this case (22) yields

$$B B_3^{-1} \Phi_{rr} = \Phi^3 + p\Phi + q \tag{24}$$

Here $p = B_1 B_3^{-1} - \tfrac{1}{3}(B_2 B_3^{-1})^2$, $q = \tfrac{2}{27}(B_2 B_3^{-1})^3 - \tfrac{1}{3} B_1 B_2 B_3^{-2} + C_1 B_3^{-1}$. Finally, we rewrite the last equation in the form:

$$B\Phi_{rr} + m^2 \Phi - \lambda \Phi^3 = C. \tag{25}$$

Here $m^2 = -pB_3$, $\lambda = B_3$ and $C = qB_3$. The equation (25) is the particular case of the equation (2). Many wave equations to some extent resemble the equation (25).

2. Let us consider an equation

$$u_{tt} = c_0^2 u_{aa} (1 + u_a^2)^{-\gamma - 1}. \tag{26}$$

If the displacement is not too great, we can approximately rewrite (26) in the form:

$$u_{tt} - c_0^2 u_{aa} = \beta u_{aa} u_a^2 + \beta_1 u_{aa} u_a^4 + k u_{aatt} \, . \tag{27}$$

Here k is a constant. We saved the nonlinear terms up to the fifth order and introduced in (27) a small phenomenological term which take into account the effect of the dispersion. Remarkably, the equation (27) contains the nonlinear terms only having the odd nonlinearity. Using (21) we rewrite the last equation in the form:

$$B_1 u_r = \tfrac{1}{3} \beta u_r^3 + \tfrac{1}{5} \beta_1 u_r^5 + B u_{rrr} + C_1. \tag{28}$$

Let

$$\Phi = u_r \ . \tag{29}$$

In this case the equation (28) yields

$$B\Phi_r{}^2 = B_1 \Phi^2 - \tfrac{1}{6} \beta \Phi^4 - \tfrac{1}{15} \beta_1 \Phi^6 - 2C_1 \Phi + C. \tag{30}$$

Let $\beta_1 \approx 0$ and a constant of integration $C_1 = 0$. In this case we have that

$$B\Phi_r{}^2 = B_1 \Phi^2 + B_4 \Phi^4 + C \, . \tag{31}$$

The equation (31) is the particular case of the equation (3). We have derived the equation that has a solution in the form of elliptic integral. In particular, these solutions describe well Euler's elastica forms. Thus, there are unidirectional travelling waves corresponding to elastica forms that have been studied by Euler. Such feature characterizes many wave equations.

3. The sine-Gordon equation is a nonlinear hyperbolic partial differential equation involving the d'Alembert operator and the sine of the unknown function. The equation, as well as several solution techniques, were known in the nineteenth century in the course of study of various problems of differential geometry. (We stress that very particular case of this equation was derived by Kirchhoff [8]. This version was used by him to model the elastica-forms). The equation grew greatly in importance in the 1970s, when it was realized that it led to solitons (so-called 'kink' and 'antikink'). The sine-Gordon equation appears in a number of physical applications, including applications in relativistic field theory, Josephson junctions or mechanical trasmission lines [36].
The equation reads

$$\Phi_{tt} - c_*^2 \Phi_{xx} + \sin\Phi = 0 \ , \tag{32}$$

where $\Phi = \Phi(x, t)$. We assume approximately that

$$\sin\Phi = \Phi - \tfrac{1}{6}\Phi^3 + \tfrac{1}{120}\Phi^3 - ... \tag{33}$$

In the low-amplitude case the equation (32) yields the Klein-Gordon equation

$$\Phi_{tt} - c_*^2 \Phi_{xx} + \Phi - \tfrac{1}{6}\Phi^3 = 0. \tag{34}$$

4. We have much interest in the Klein-Gordon's equation. This equation will be considered attentively in the next sections. Here we note that this equation is usually presented in the following form

$$\Phi_{tt} - c_*^2 \Phi_{xx} + \partial V / \partial\Phi = 0, \tag{35}$$

V is the potential [36]:

$$V = -\tfrac{1}{2} m^2 \Phi^2 + \tfrac{1}{4}\lambda\Phi^4 + \tfrac{1}{6}\lambda_6\Phi^6. \tag{36}$$

Here c_*, m^2 , λ and λ_6 are constants. We substitute (36) in the equation (35). As a result it gives

$$\Phi_{tt} - c_*^2 \Phi_{xx} = m^2\Phi - \lambda\Phi^3 - \lambda_6\Phi^5. \tag{37}$$

Waves having complex elastica-like profiles are the main interest of this research. The volume of the paper does not allow to study attentive these waves for all strongly-nonlinear wave equations. However, the volume allows to show existence of this class strongly-nonlinear waves on examples of considering noted above wave equations.
As the most important example we consider one-dimensional nonlinear Klein-Grdon equation describing so-called Φ^4 scalar field (see, for example, (34)). We write this equation in the form

$$\Phi_{tt} - c_*^2 \Phi_{xx} + m^2\Phi - \lambda\Phi^3 = 0. \tag{38}$$

New coordinates *r* and *s* are introduced

$$r = ct - x, \quad s = ct + x. \tag{39}$$

In this case the equation (38) is rewritten in the form:

$$(c^2 - c_*^2)(\Phi_{rr} + \Phi_{ss}) + 2(c^2 + c_*^2)\Phi_{sr} = -m^2\Phi + \lambda\Phi^3. \qquad (40)$$

For one hand travelling waves the last equation yields

$$(c^2 - c_*^2)\Phi_{rr} + m^2\Phi - \lambda\Phi^3 = 0. \qquad (41)$$

The equation (41) is the particular case of the equation (2) and (41) practically coincides with (25). We can rewrite the equation (41) in the form:

$$\Phi_r{}^2 = \tfrac{1}{2}\lambda(c^2 - c_*^2)^{-1}(\Phi^4 - 2\lambda^{-1}m^2\Phi^2 + 4\lambda^{-1}C). \qquad (42)$$

Here C is a constant of integration. This equation practically coincides with (9).

5. Many of wave equations may be simplified to (41) form. Let us consider the Gardnet equation. This the cubic nonlinear equation is written here in the usual dimensionless form [36a]

$$u_t + 6uu_x + 6u^2u_x + u_{xxx} = 0. \qquad (42a)$$

It is known that the linear transformation

$$\Phi = u(x - \tfrac{3}{2}t, t) + \tfrac{1}{2} \qquad (42b)$$

simplifies a solution of (42a) to the solution of the modified Korteweg-de-Vries equation

$$\Phi_t + 6\Phi^2\Phi_x + \Phi_{xxx} = 0. \qquad (42c)$$

For unidirectional waves the equation (42c) yields

$$\Phi_{rr} - c\Phi + 2\Phi^3 = C. \qquad (42d)$$

This equation practically coincides with (41). The equation (41) may be transformed to (42) form.

Solutions of the equation (42) will be considered in the following section.

2.2. Examples of exact solutions describing the elastica-like waves

1. Let in (42)

$$\tfrac{1}{2}\lambda(c^2 - c_*^2)^{-1} = -1, \quad \lambda^{-1}m^2 = -2c \quad \text{and} \quad B^2 = \lambda^{-2}m^4 - 4\lambda^{-1}C. \qquad (43)$$

In this case we can rewrite the equation (42) in the form:

$$\Phi_r{}^2 = B^2 - (\Phi^2 + 2c)^2. \qquad (44)$$

Solutions built using elliptic functions. The cases may be classified as follows:

1.1. $c = -1$ and $B = 2$

Fig.21. Euler's soliton (see, also, Figs. 1, 14) [33].

It is easy to see that this figure corresponds well to Euler's figure 10 in Fig. 1.

1.2. $c=-1$ and $0<B<2$

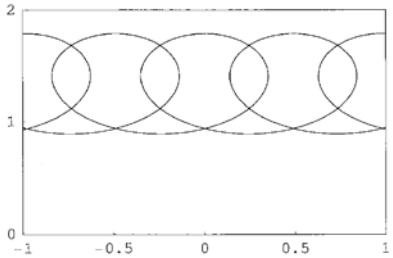

Fig.22. The elastica form modelling the case $\lambda=0.2$ in Fig. 2 (right) [33].

It is easy to see that this figure resembles Euler's figure 11 in Fig. 1.

1.3. $c=-1$ and $B>2$

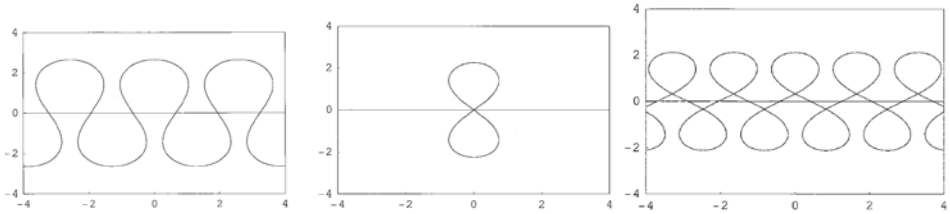

Fig. 23. The elastica forms modelling the cases $\lambda=0.4,\ 0.3027$ and 0.28 in Fig. 2 (right) [33].

It is easy to see that Fig. 23 corresponds well to Euler's figures 7, 8, 9 in Fig. 1. We have shown that the Klein-Gordon equation describes the elastica-like forms. Thus, the different elastica-like waves can be in the scalar fields.

2. Perhaps, we will be able to describe wider spectre of the the elastica-like forms, if the nonlinear Klein-Gordon equation to present as the Kirchhoff-like equation (11). First we rewrite (42):

$$\Phi_r^{\,2}=\tfrac{1}{2}\lambda(c^2-c_*^2)^{-1}(\Phi^2-\Phi_+^2)(\Phi^2-\Phi_-^2). \tag{45}$$

Here Φ_+^2 and Φ_-^2 are roots of the equation $\Phi^4-2\lambda^{-1}m^2\Phi^2+4\lambda^{-1}C$. Let (Fig. 13)

$$\Phi=\Phi_+\sin\theta \ \text{ and } \ \Phi_r=\Phi_+\theta_r\cos\theta. \tag{46}$$

In this case

$$\theta_r^{\,2}=\tfrac{1}{2}\lambda(c^2-c_*^2)^{-1}\Phi_-^{\,2}(1-\Phi_+^{\,2}\Phi_-^{\,-2}\sin^2\theta). \tag{47}$$

Finally the equation (47) may be presented as the following

$$\theta_x^{\,2} + R(\cos\alpha - \cos\theta) = 0\,. \qquad (48)$$

We stress that Love [2] studied many Euler's elastica using the equation (48).

3. It is possible to give different interpretations of the results presented above. This possibility quite corresponds to the main objective of science – the creation of the overall picture of the world surrounding us. The picture should be painted from some general positions. Indeed, Nature is uniform, therefore all divisions in science are the conditionality to some extent. In principle, many results received in one knowledge domain can be useful and in other areas of science. Future of mankind is connected not only to study of elementary particles or the evolution processes, but first of all with an exchange of information which has been accumulated in different areas of science.

It is known that physical processes of generation and transformation of waves can differ dramatically , nevertheless equations and analytical solutions describing these processes are often similar. For example, shock-, soliton – and cnoidal –like solutions are well known in nonlinear dynamics.

Taking into account the above, we pay special attention to nonlinear Klein-Gordon equations. On the one hand, these equations describe the wide range of nonlinear waves. These waves are often used to describe the wave processes in the very early universe [37, 38]. On the other hand, these equations are widely used for modeling of massless particle nucleation. Apparently, nonlinear Klein-Gordon equations serve as a bridge allowing to link the cosmic objects and elementary particles by wave analysis. Such consideration is necessarily for modeling the origin of the Universe. Thus, it is possible that the eastica-like solutions of the nonlinear Klein-Gordon equation (NKGE) will shed an additional light on the mystery of the origin of the Universe.

This equation cannot be straightforwardly interpreted as a Schrödinger equation for a quantum state, because it is second order in time. Still, with the appropriate interpretation, it does describe the quantum amplitude for finding a point particle in various places, but the particle propagates both forwards and backwards in time. Any solution to the Dirac equation is automatically a solution to the Klein–Gordon equation, but the converse is not true.

The subsequent part of our study considers approximate solutions of NKGE and the interpretation of these solutions to simulate this origin.

3. Elastica-like approximate solutions of an inhomogenuous nonlinear Klein-Gordon equation describing the eruption of the Universe out of a pre-universe

Can NKGE describes the origin of the Universe? On the whole, an idea of using scalar equations is well known in cosmology [39]. Practically, all cosmologists use scalar fields in their theories. Recent results from the Planck satellite, combined with earlier observations from WMAP, ACT, SPT and other experiments do not support the current standard model of cosmology, which combines the Big Bang origin and the inflationary scenario [39-41]. The origin of the Universe may be described by the scalar fields since the recent observations favour cosmological models with simple scalar fields. In particular, eruption of the Universe out of a pre- universe was studied with the help of NKGE in [19, 35, 42].

In this section of approximate solutions of NKGE are presented describing the evolution of pre -universe into the very early Universe, where gravitational forces have not yet emerged.

3.1. 'Long' quantum actions

Here we present the extract from [17] which deals with the results of the action of the quantum perturbation on some element of a multidimensional pre-universe. As a result this element receives enough energy so that to erupt from the pre-universe. This element of the scalar field forms our Universe. A rather complex profile of the quantum perturbation is used. This leads to the fact that the process of eruption of the Universe is quite complex, and may be accompanied by the generation of the elastica-like forms (waves).

The most simplified model NKGE is used. According to section 1.2.2 NKGE is simplified to an algebraic equation having the following form

$$\Phi^3 + \bar{R}\Phi = \lambda^{-1} f(\xi). \tag{49}$$

Here $\bar{R} = -\lambda^{-1} m^2$ [17], $f(\xi)$ describes the quantum action, variable ξ is determined by number of space dimensions of the pre-universe and time. The equation (49) has three solutions. These solutions can determine three real scalar fields. It is known, that many physical fields can exist simultaneously at the same place. At the same time they do not practically interact with each other. However, due to quantum fluctuations the fields can occasionally interact if there are certain critical (resonant) situations. Below several examples of the quantum action are presented.

Let us study a case of the quantum fluctuations having long enough duration (Fig. 24). It is assumed also that the quantum action function can have a fast varying part. This part is much shorter of the action duration. Examples of similar actions are shown in Fig. 24 (centre and right).

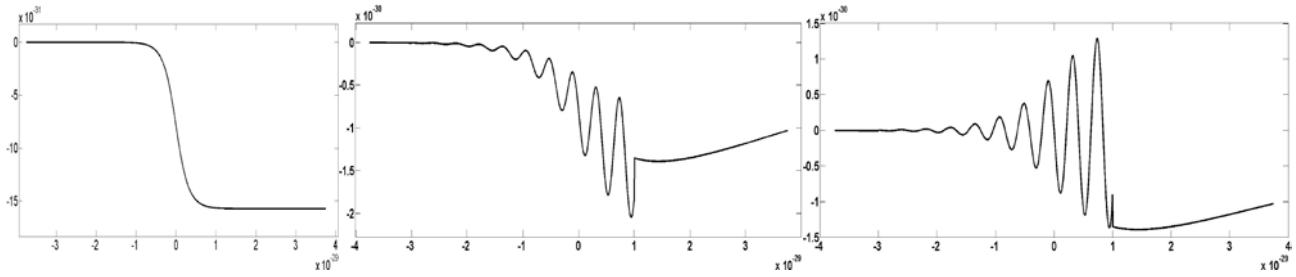

Fig. 24. The quantum action described by the expression $\lambda^{-1} f(\xi) = \tilde{A} \arg\tan[\exp(-\Omega\xi)]$ (left) and more complex curves describing the quantum action in (49) (centre and right).

The solutions of the equation (49) obtained for the above quantum actions are presented in Figs. 25-28. Considering these figures we mean that the roots 1 and 2 (the segments 1 and 2) of the equation (49) describe the evolution of certain scalar fields 1 and 2.

1. First it is assume that $\lambda^{-1} f(\xi) = \tilde{A} \arg\tan[\exp(-\Omega\xi)]$ (Fig. 24 left), where $\tilde{A} = A \cdot 10^{-30}$, $\Omega = 5 \cdot 10^{29}$ and $\overline{R} = -10^{-20}$ in (49). For this case the solutions are shown in Fig. 25. It is seen that the scalar fields are independent if A=0.01 or A=0.2 in $\tilde{A} = A \cdot 10^{-30}$. The segments (fields) 1 and 2 begin to interact when A=0.245. The jumps of the scalar fields (segments 1 and 2) to the positive values take place when A>0.246.

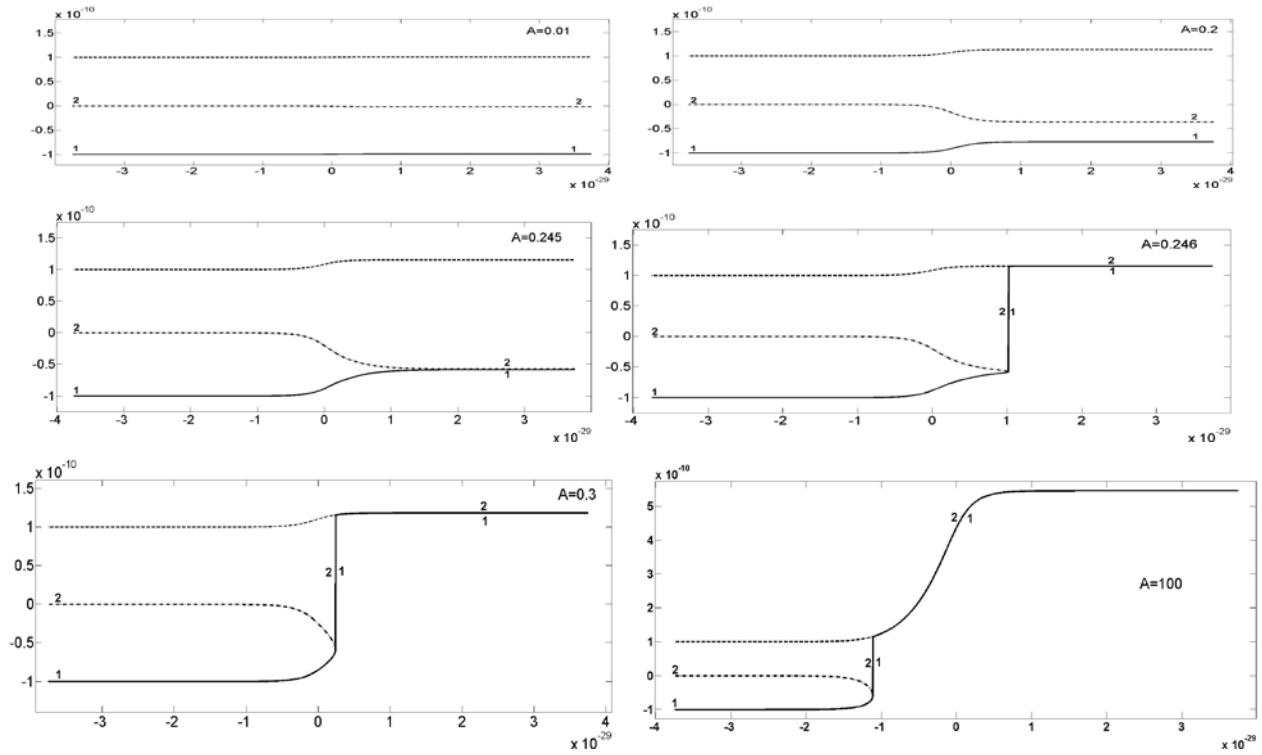

Fig. 25. Results of the quantum action $\lambda^{-1} f(\xi) = A \cdot 10^{-30} \arg\tan[\exp(-\Omega\xi)]$ (Fig. 24 left) calculated for different coefficient A. The scalar fields 1 and 2 can jump up to the top level (the plateau) if $A \geq 0.246$.

We have considered the case (Fig. 24 left) when a long quantum action is not accompanied by quantum fluctuations of small amplitude. It is known [17] that their impact can be very important. These fluctuations determine the possibility of the destruction of the spacetime of the pre-universe. On the other hand the small fluctuations can influence on the eruption of the scalar field from the potential well. Below we present the results of the analysis of the impact of the small fluctuations on the studied nonlinear processes.

2. Let us consider the quantum fluctuation presented in Fig. 24 (centre and right). The amplitude of the quantum fluctuation $\lambda^{-1} f(\xi)$ equals 10^{-30} and $\overline{R} = -10^{-20}$ in (49). Some results of the calculations are presented in Fig. 26. Curves A were calculated for the action presented qualitatively in Fig. 24 (centre). Curves B were calculated for the action presented qualitatively in Fig. 24 (right).

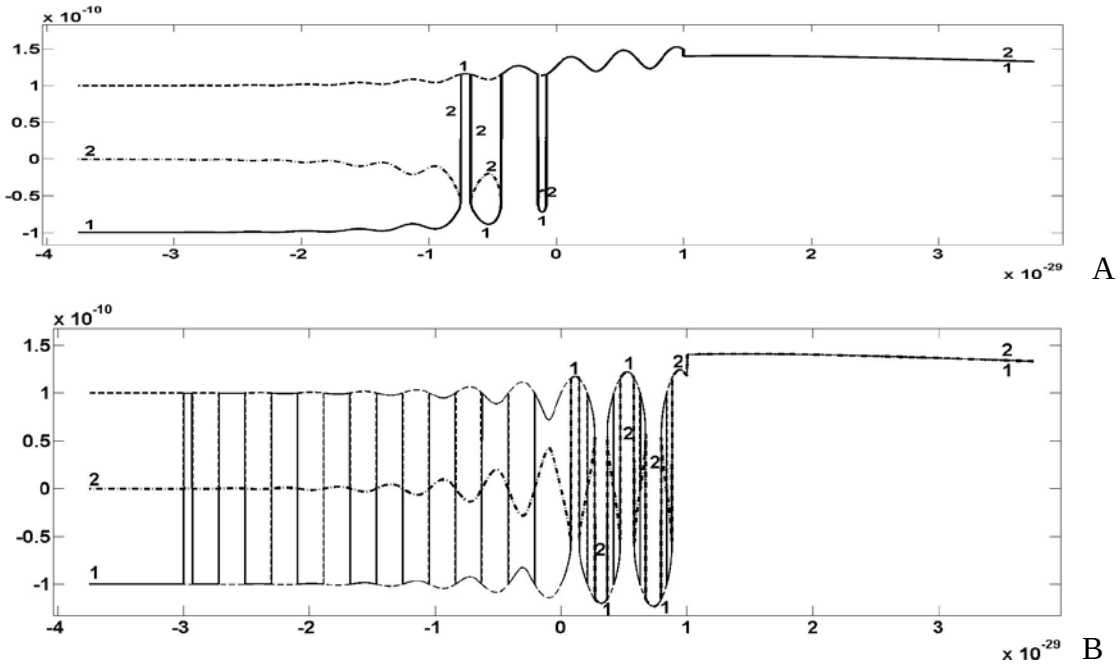

Fig. 26. Results of the quantum actions. The actions are accompanied by quantum oscillations of a small amplitude (see Fig. 24 (centre and right)).

Fig. 26 demonstrates the existence of three scalar independent fields when the horizontal coordinate is smaller -10^{-29}. These fields interact very strongly within an interval from -10^{-29} to 0 (A) and from 0 till 10^{-29} (B). The single composite field is formed after the interaction. Perhaps, this field corresponds to the origin of the Universe. The formation of the mushroom-like (elastica-like) structure [17] is shown in the picture B. This structure is a result of the strongly nonlinear interaction of the initially independent scalar fields. This structure resembles Fig. 7 of Euler (Fig. 1).

3. The above we have considered cases when the coefficient $\overline{R}$ in (49) was very small. Now we study

additionally cases when this coefficient is $\bar{R} = -10$ or $\bar{R} = -10^{20}$.

3.1. Let us consider the case of the quantum action which is similar to the case presented in Fig. 24 (centre). The calculation results are shown in Fig. 27.

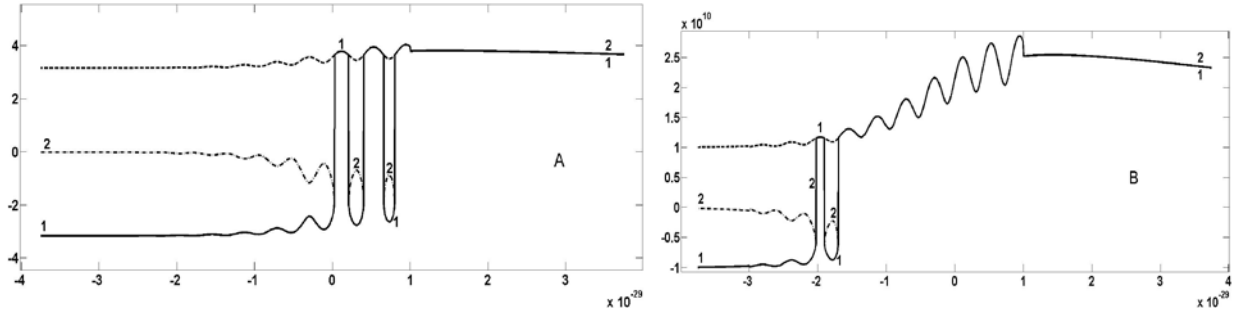

Fig. 27. Results of the quantum actions accompanied by quantum oscillations of a small amplitude.

Here the curves A are calculated for $\bar{R} = -10$ and the amplitude of the quantum fluctuation $\lambda^{-1} f(\xi)$ equals $10^{1.1}$. Curves B are calculated for $\bar{R} = -10^{20}$ and the amplitude of the quantum fluctuation $\lambda^{-1} f(\xi)$ equals 10^{31}. In these cases we found the resonant parameters at which the three initial independent scalar fields begin to interact and form a new composite field.

3.2. Let us consider the case of the quantum action which is similar to the case presented in Fig. 24 (right). The calculation results are shown in Fig. 28.

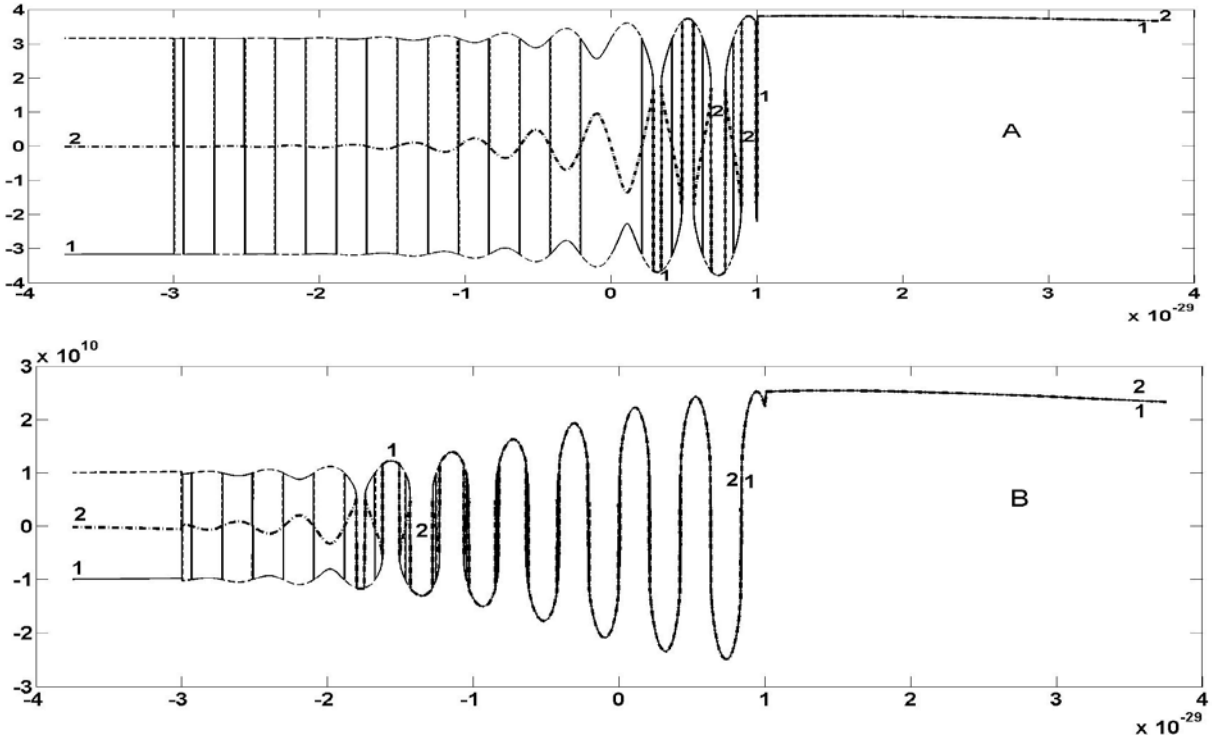

Fig. 28. Results of the quantum actions accompanied by quantum oscillations of a small amplitude. The amplitude of the quantum fluctuation $\lambda^{-1} f(\xi)$ equals -10^{-30}. The formation of the mushroom-like (elastica-like) structure [17] is shown. This structure resembles Fig. 7 of Euler (Fig. 1) and the forms $\lambda = 0.35, 0.4$ and 0.5 (see Fig. 2).

Here the curves A are calculated for $\overline{R} = -10$ and the amplitude of the quantum fluctuation $\lambda^{-1} f(\xi)$ equals $10^{1.1}$. Curves B are calculated for $\overline{R} = -10^{20}$ and the amplitude of the quantum fluctuation $\lambda^{-1} f(\xi)$ equals 10^{31}. We found the resonant parameters at which the three initial independent scalar fields begin to interact and form a new composite field.

Conclusion. We found the resonant parameters at which the three initially independent scalar fields begin to interact by means of multivalued discontinuous oscillations. As the result the new field is generated which is thrown on the plateau-like top of the hill (see Figs. 25-28). We think that similar new composite fields may be considered as a starting point of the evolution of the Univerve. We studied the instability of a scalar field which is caused by a quantum fluctuation.

The amplitude of the composite field oscillations increases beyond that of the original fields. It may increase up to a point when the scalar field element escapes from the potential well. Because of the oscillations this process is described by the composite (multivalued) and discontinuous curves which resemble some elastica forms of Euler. We assume that this process corresponds to the origin of the Universe [17, 19, 35, 42].

Thus, by the way of analytic solution of the nonlinear Klein-Gordon equation we come to the initial point of some models of the origin of the Universe. In particular, the existence of some volume of the inflaton on the top of a certain energetic hill is the starting point for a few inflation models [39, 40].

3.2. The fragmentation of multidimensional spacetime during the field eruption from the potential well

We have studied the great amplification of quantum fluctuations of a scalar field. In particular, discontinuous oscillations of the fields occur. These oscillations can work like certain hammer blows, smashing the local spacetime on some fundamental blocks. These blocks may differ from our ideas about the basic elements of spacetime. Their sizes may depend on the energy of the oscillations (the energy of the hammer blows). In particular, it is accepted in [17, 19, 35] that the spacetime of the multidimensional pre-universe may be fragmented into some one-dimensional string-like ingredients.

The multivalued and discontinuous oscillations of the composite field include the elements of the previously-independent fields (see figures of the section 3.1). The transition of one element to another is not necessarily smooth and continuous. The discontinuities could destroy the spacetime. The boundaries between spacetime dimensions were less stable during the eruption than they are now. As a result the multidimensional spacetime can be split into many two-dimensional (space + time) elements. The spacetime fabric was transformed and fragmented when the field energy has been increased strongly. Generally speaking, it agrees with the 'vanishing dimensions' theory [43-46]. According to this theory, systems with higher energy have a smaller number of dimensions. The higher the energy, the smaller spacetime dimensions. Thus, our theory implies that the number of dimensions in the Universe reduced during the eruption.

Generally speaking, the initial energy field could have many dimensions. The string theory proclaims that the number of the dimensions may be different, for example, 5, or 11 or 26. As the number of dimensions reduces, the volume of the initial energy element (bubble, clot, sphere, drop) can increase after the fragmentation very, very strongly.

The process could be visualised by imagining a three-dimensional drop of oil impacting the surface of water. As a result of the impact the oil drop is separated into many elements (particles) which spread over the two-dimensional surface of water. These elements of oil occupy in the two-dimensional space much bigger volume than they had in the initial moment. It is important that the elements became more isolated from each other comparing to when they were inside the drop.

Qualitatively the fragmentation of the spacetime fabric could resemble the atomization of the water drop (see Fig. 9). The fragments (elements) gained extremely high energy. It was assumed [17, 19, 35] that the elements became absolutely isolated without any connections.

On the whole this conclusion agrees with suggestions of Steven Carlip of the University of California, Davis [46]. In 2012 he gathered up many theories and found that, according to many of them, the Universe had got one or two spatial dimensions during the hot, dense start. In other words, geometry appears to have been radically different in the beginning. Carlip and his colleagues showed that space was split into discrete elements in the first seconds of the Universe. Each element experiences nothing outside its own existence. Thus, the behaviour of the Universe's spacetime might be very surprising in the beginning.

3.3. The elastica-like waves and a resonant model of the origin of elementary particles

We mainly considered the unidirectional waves. Now we consider the strongly-nonlinear one-dimensional waves travelling in opposite directions. We will continue to study NKGE for this case. The scalar field function Φ is represented as a sum:

$$\Phi = \Phi^{(1)} + \Phi^{(2)}, \tag{50}$$

where $\Phi^{(1)} >> \Phi^{(2)}$. In this case the equation (40) yields

$$\begin{aligned}&(c^2 - c_*^2)[(\Phi^{(1)} + \Phi^{(2)})_{rr} + (\Phi^{(1)} + \Phi^{(2)})_{ss}] + 2(c^2 + c_*^2)(\Phi^{(1)} + \Phi^{(2)})_{sr} \\ &= -m^2(\Phi^{(1)} + \Phi^{(2)}) + \lambda(\Phi^{(1)} + \Phi^{(2)})^3.\end{aligned} \tag{51}$$

Here c is a constant. Let its value is very close to c_*,

$$c = c_* + \overline{c}, \tag{52}$$

where $\overline{c}$ is the perturbation of the speed c. It is assumed that

$$\Phi^{(1)} = J(r) - J(s) \text{ and } \Phi^{(2)} = j(r) - j(s). \tag{53}$$

Thus, we will not take into account the interaction of the opposite travelling waves. Taking into account (50), (52) and (53) we split (51) to two equations

$$2(c^2 + c_*^2)(\Phi^{(1)} + \Phi^{(2)})_{rs} = 0, \tag{54}$$

$$\begin{aligned}&[2c_*\overline{c}(\sum_{i=1}^{I} k_i^2)^{0.5} + \overline{c}^2][(\Phi^{(1)} + \Phi^{(2)})_{rr} + (\Phi^{(1)} + \Phi^{(2)})_{ss}] \\ &+ m^2(\Phi^{(1)} + \Phi^{(2)}) - \lambda(\Phi^{(1)} + \Phi^{(2)})^3 = 0.\end{aligned} \tag{55}$$

We consider oscillations of the field inside of some resonator. At the ends of it

$$\Phi = 0 \text{ at } x = 0; L. \tag{56}$$

Let

$$\Phi^{(1)} = A(\sin \omega c^{-1} r - \sin \omega c^{-1} s) \text{ and } \omega L c^{-1} = 2\pi N \quad (N = \pm 1, \pm 2, \pm 3, \ldots) \tag{57}$$

It is also suggested that the function j is periodical having the period equal L. In this case the conditions (56) and equation (54) are satisfied. Let us now consider (55). We will construct the approximate solution of (55) which is valid where

$$\Phi^{(1)}{}_{rr} >> \Phi^{(2)}{}_{rr} \quad \text{and} \quad \Phi^{(1)}{}_{ss} >> \Phi^{(2)}{}_{ss}. \tag{58}$$

In this case equation (55) yields

$$j^3 + \overline{R} j + q \sin \omega c^{-1} r = 0, \tag{59}$$

where

$$\overline{R} = -m^2 / \lambda, \; q = [2c_*\overline{c} + \overline{c}^2]\lambda^{-1}\omega^2 c^{-2} A. \tag{60}$$

There are three distinct cases, when the equation (59) has real solutions:

1. Let $\overline{R} = 0$, then the equation (59) is satisfied if

$$j = (-q)^{1/3}. \tag{61}$$

2. Let $\bar{R}>0$, then the function j is unique, single-valued and continuous

$$j = -2D\sinh[\tfrac{1}{3}\operatorname{arcsinh}(0.5qD^{-3})], \tag{62}$$

where $D=[sign(q)](|R|/3)^{0.5}$.

3. Let $\bar{R}<0$ and $q^2/4+R^2/27\le 0$. In this case there are three solutions

$$j_M = -2D\cos[\tfrac{1}{3}\arccos(0.5qD^{-3})+2M\pi/3], \tag{63}$$

where M =0;1;2. Using these continuous solutions we can construct multivalued solutions which can describe some elatica-like forms (waves).

3.3.1. The origin of the particles

For model calculations we assume in (59) that

$$\bar{R}=-0.0014,\ \omega=25.5,\ c=1 \text{ and } q=0.0001. \tag{64}$$

1. First we study the nonlinear oscillations described by the equation (59) and $\Phi^{(2)}$ (53). Figs. 29 and 30 illustrate second and first modes of the oscillations correspondingly.

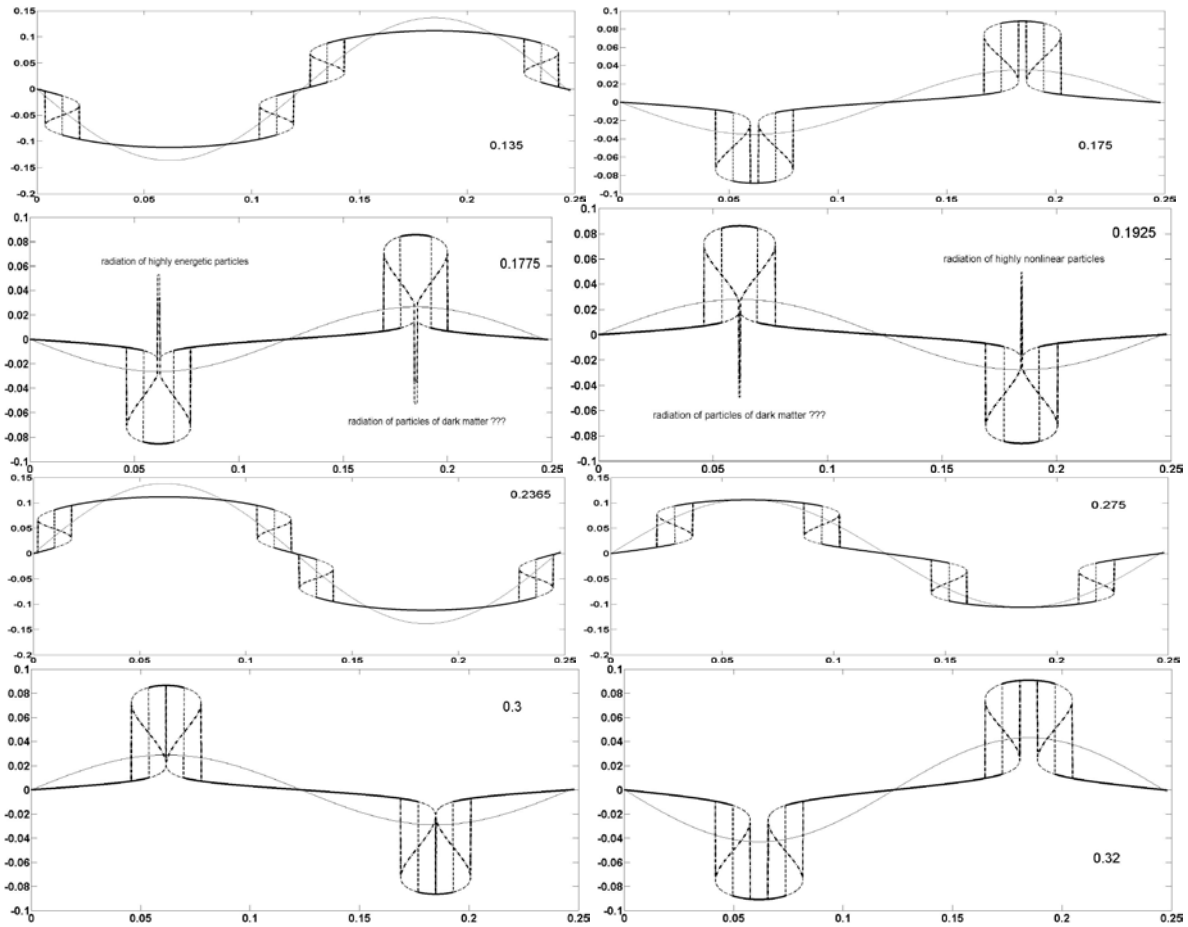

Fig. 29. Resonant continuous oscillations of the scalar field elements according to the second resonant form. Periodic formation of the particles of matter. The thin smooth lines correspond to the linear oscillations [19, 35]. The forms 0.175 and 0.3 resemble Fig. 9 of Euler (Fig. 1).

We think that Fig. 29 illustrates the emergence of particles of energy and matter. The particles radiate above or below the scalar field element. Namely, there are moments (for example, 0.1775 and 0.1925) when the particles separate from the energy level of the element.

It is important that the appearance of the energetic particles (see Fig. 29) incorporates an important quantum concept - the momentary creation of pairs of particles. However, periodic radiation of a sole particle is also possible if the element oscillates according to the first resonant form (Fig. 30). For the calculations of curves of Fig. 30 we used (64) where $\omega = 26.1$.

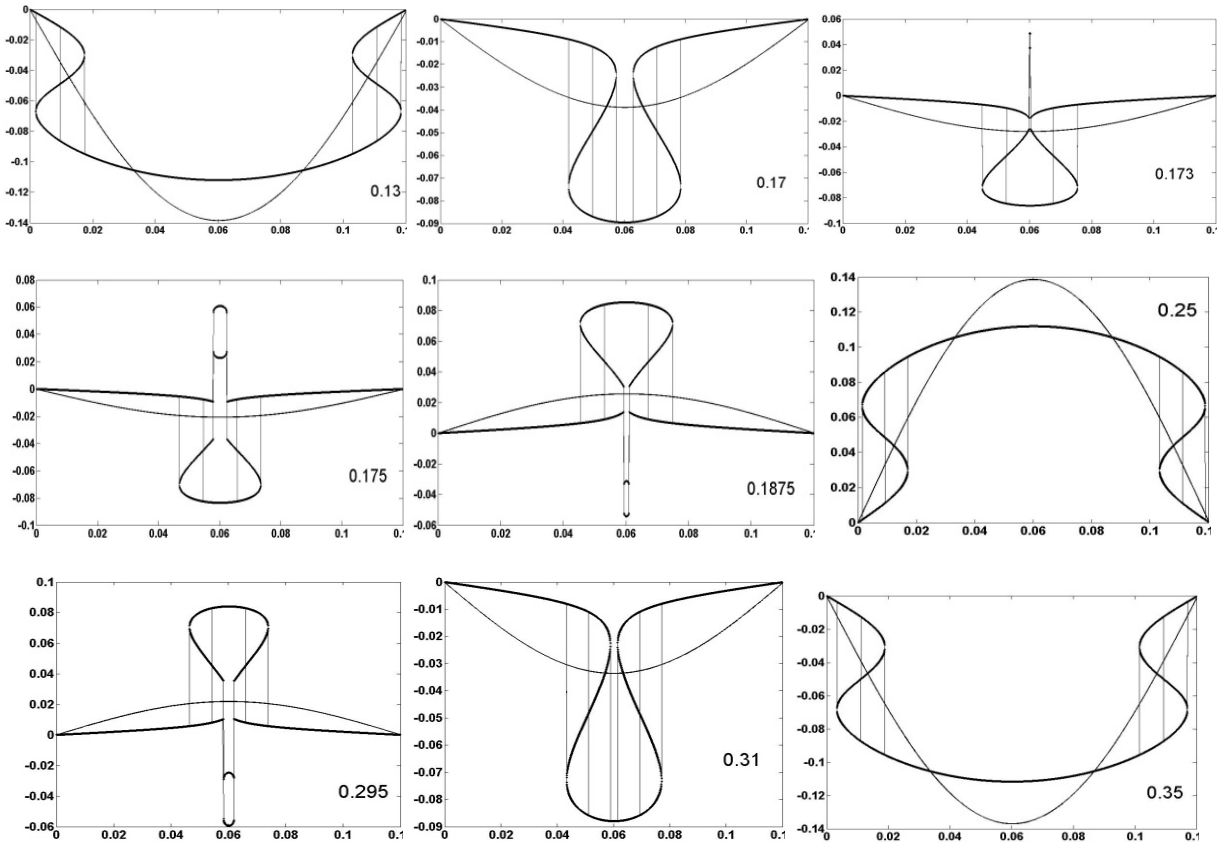

Fig. 30. Resonant oscillations of the scalar field elements according to the first resonant form. Periodical formation of particles of matter. The thin smooth lines correspond to the linear oscillations [19, 35]. Presented forms resemble Figs. 7 and 10 of Euler (Fig. 1).

The shapes of the nonlinear oscillations are quite different from the linear forms. In particular, the nonlinear shapes have the folds which were formed by the curved segments corresponding to the different solutions of the

equation (59). Within and near these folds the scalar field can have jump discontinuities. There the differential can be very large up to infinite values since the gradient determines the density and the pressure of scalar fields.

Taking into account Figs. 29 and 30 we can imagine that very massive particles may be generated during the resonant oscillations of the fragments of the scalar field.

2. Then we calculate the scalar field oscillations taking into account the linear contribution. The oscillations are determined by expressions (50), (53) and (57):

$$\Phi = A[\sin(\omega c^{-1} r - \pi/2) - \sin(\omega c^{-1} s - \pi/2)] + j(r) - j(s). \qquad (65)$$

We have assumed that the shift of the linear oscillations (linear component of the solution) relative to the nonlinear oscillations (nonlinear component of the solution) at the resonance is $-\pi/2$.

Thus, the scalar field oscillations are determined by expressions (65) and parameters (64). The results of the calculation are presented in the Fig. 31.

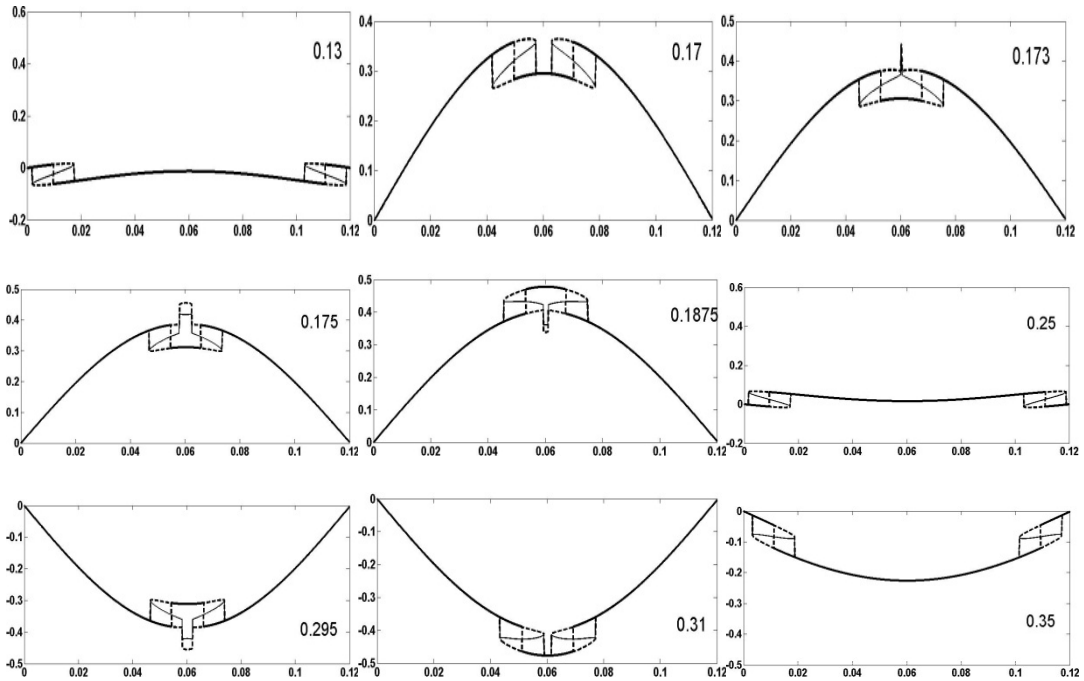

Fig. 31. Resonant oscillations of a fragment of the scalar field. The first resonant form [19, 35].

The results of the calculations are qualitatively corresponded to the experiments [28] (see Figs. 13 and 32). In particular, the curves 0.13, 0.17 and 0.173 (Fig. 31) describing the peak (jet) formation correspond to the photos of Fig. 32 (left). The curves 0.25, 0.295, 0.31 and 0.35 (Fig. 31) describing the evolution of the wave trough correspond the photos of Fig. 32 (right).

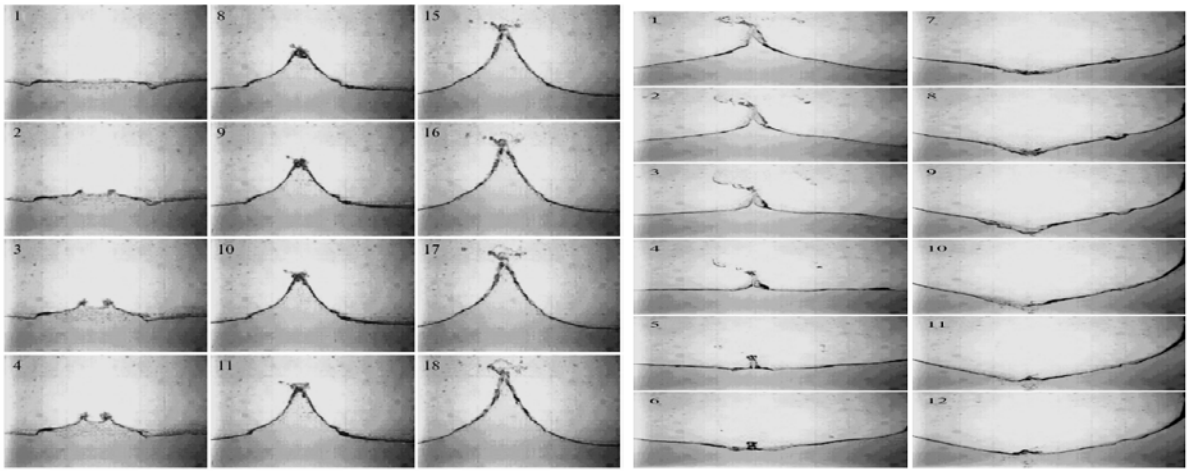

Fig. 32. Experimental data [28].

The elements of scalar field noted above vibrate according to their resonant frequencies and can radiate particles of energy. If these particles of the scalar field possess some critical energy, they form matter [19, 35].

3.3.2. The origin of dark and normal matters, and dark energy

We can imagine that during the oscillations and the radiation of the energy particles the common energy of the fragment is reduced. Let us study this phenomenon.

Dark matter particles. First we assume that $\overline{R} = -m^2\lambda^{-1} = -0.0014$, A=-0.2, $\omega = 26.1$, $L = 0.12$, c=1 and $q = 0.0001$. The results of the calculations are shown below.

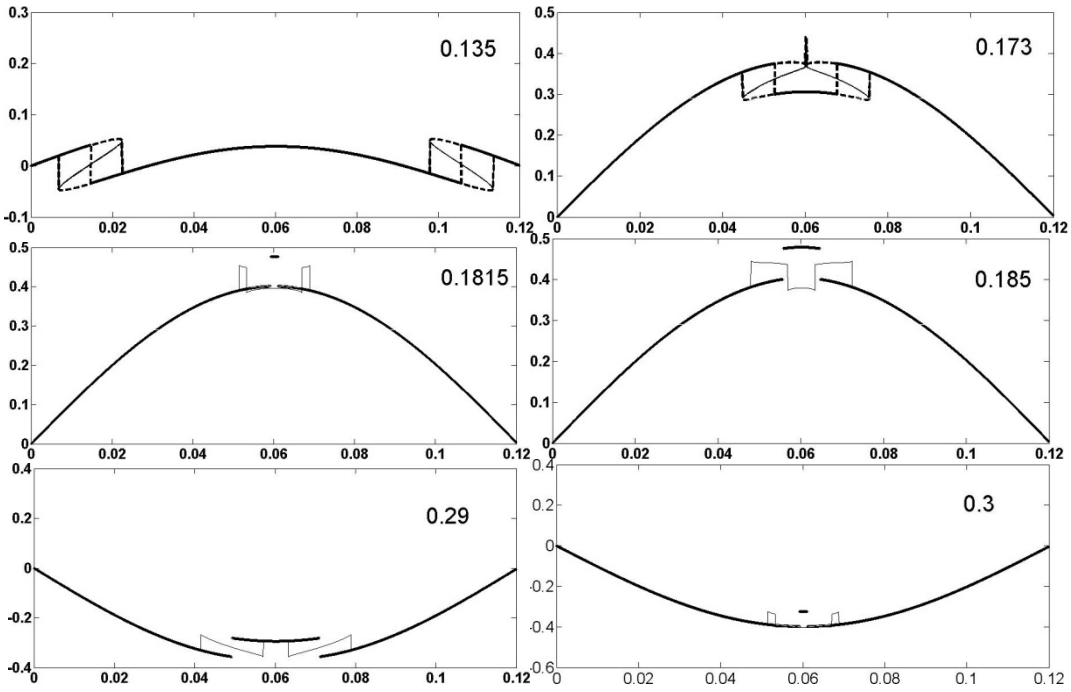

Fig. 33. Resonant oscillations of a fragment of the scalar field accompanied by eruptions of energetic particles. The case of $\overline{R} = -m^2\lambda^{-1} = -0.0014$ [19, 35]

On the whole we have got the results which are similar presented in Figs. 29-32. We assume that they describe the formation of very heavy particles.

Normal matter particles. Increasing $\overline{R} = -m^2\lambda^{-1} = -0.00042$ we receive the results shown in Fig. 34.

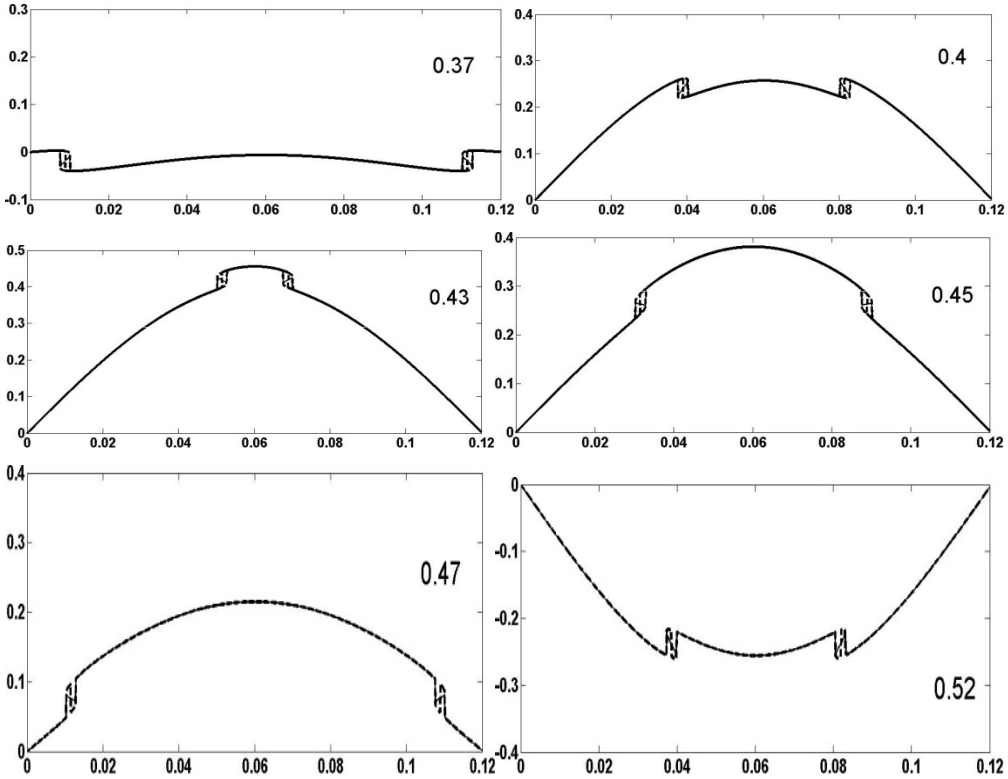

Fig. 34. Resonant oscillations of a fragment of the scalar field. The case of $\overline{R} = -m^2\lambda^{-1} = -0.00042$ [19, 35].

We assume that Fig. 34 describes the formation of normal matter particles.

Dark energy particles. One can see that Fig. 34 does not show the particle radiation clear. However, we assume that the energy of the fragment continues the reducing. Therefore, we assume that the coefficient $\overline{R} = -m^2\lambda^{-1} = -0.0000014$. Corresponding oscillations are shown in Fig. 35.

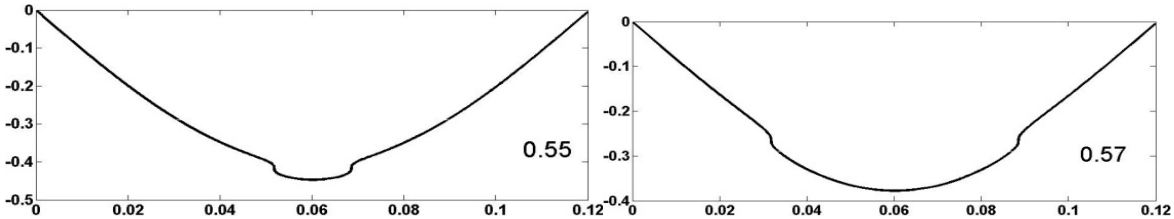

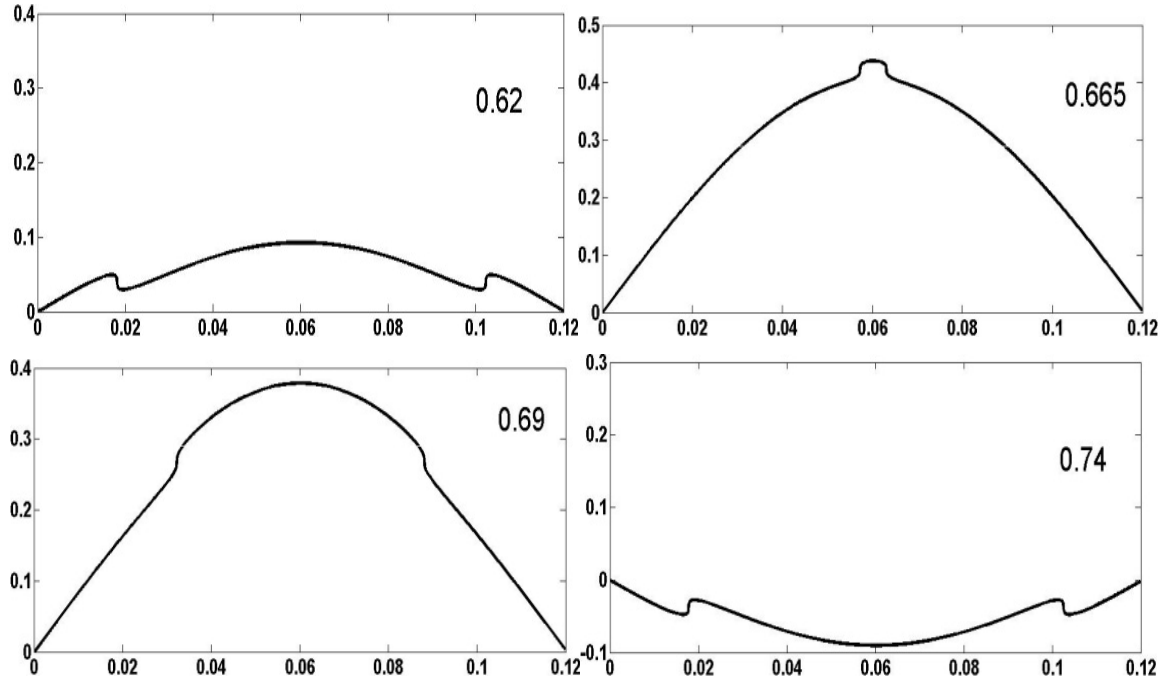

Fig. 35. Resonant oscillations of a fragment of the scalar field. The case of $\overline{R} = -m^2\lambda^{-1} = -0.0000014$ [19, 35].

It is known [39] that the density and the pressure depend very strongly on the gradient of a scalar field. In points where the field changes rapidly the pressure and the density can be very large. In particular, the mass of the dark matter particles may be very near infinite, the mass of the normal matter particles may be extreme large, but the mass of the dark energy may be very small.

We assume that highly energetic particles (Figs. 29-31 and 33) could be very stable. These particles may correspond to the dark matter. We can imagine that these particles had been stable for billions of years before they begun to decay. The last process can determine the law of expansion of the modern Universe [17, 19, 35]. The particles radiated near the resonances can form the normal matter. They could begin to work like a scaffold creating the cosmic structure. The dark energy is spread within this structure.

Important conclusion. Thus, the calculations (Figs. 29-31 and 33) have shown that the radiation of the particles is possible only for sufficiently small values of the transresonant parameter $\overline{R}$. They might be formed only far enough from the exact resonances. On the other hand, we get almost harmonically oscillating elements of energy if $\overline{R} \cong 0$ (Fig. 35). We can assume that these elements correspond to the dark energy. Thus, this energy is a remnant of the initial energy of the fragments (elements). The remnant was stored after the transresonant transition.

The very energetic particles (Figs. 29-31 and 33) correspond to the dark matter. The less energetic particles after the collapse into more elementary elements (the normal matter) could form our visible universe. According to the presented model, the transresonat process has determined the formation and

contents of the matters and energies in the Universe. During this process the pure energy of the Universe was reducing, since the matter was appearing. According to this model the origin of the Universe might consist from five stages:

1. The eruption of the energetic bubble out of the pre-universe and the fragmentation of the spacetime of this bubble. The fragments of the spacetime of the bubble are completely independent;

2. Radiation of energetic resonant particles by the fragments;

3. The dark matter began to form when the fragment frequency crosses the boundary of the resonant band (when $\overline{R} = -\lambda^{-1} m^2$ crosses the boundary of the resonant band);

4. The normal matter began to form when $\overline{R}$ increases enough;

5. The initial energy stops the transforming into energetic particles. It is a case of practically exact resonance, when $\overline{R} \approx 0$ and $\overline{R} < 0$. We have $m^2 \approx 0$.

6. Density of the dark energy begins to drop to zero [49].

4. Supporting experimental results: gravity waves

In the subsection 2.2 and the section 3 we presented many examples of the oscillations of a scalar field. Do they describe the behaviour and evolution of the fundamental field of the pre-universe? We do not have experimental evidence supporting or denying this statement.

However, it is possible to expect that the above waves can exist in the case of other wave processes, since the wave processes are described by similar equations. The above we showed that there are certainly analogies in the wave processes of different physical nature. Folded shapes of the scalar field waves are complex. However, similar evolution was observed on the surfaces of liquids. Thus, the scalar field waves can be similar to the waves in water. Let us continue this analogue at this section.

4.1. Strongly-nonlinear Faraday waves

Here we refer to a more conventional example of gravity surface waves to support the above findings for scalar resonant waves. In recent years, very interesting results of the study of vertically-excited resonant waves have been received. These waves can be named as Faraday's strongly-nonlinear waves [16].

Let us compare waves of Figs. 33-35 with experimental waves presented in Fig. 36. These waves were excited in a vertically oscillating container. Its length was 0.6 m, and the width 0.06 m. The depth of water was 0.3 m. All wave profiles (Fig. 36) were observed during one experiment. The forcing frequency was 1.6 Hz and the amplitude was 4.6 mm.

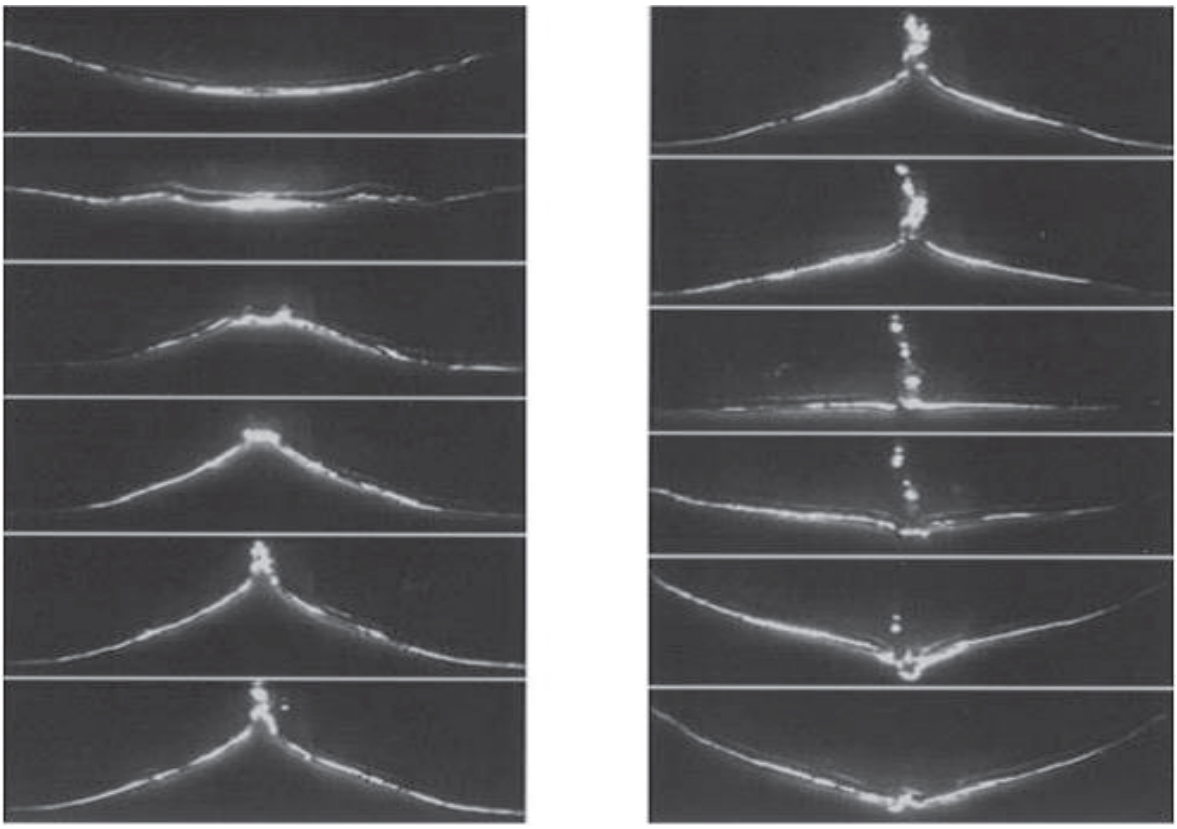

A. Gravity waves observed at the moments of time: 0, 0.04, 0.08, 0.12, 0.16, 0.2 (left), 0.24, 0.28, 0.32, 0.36, 0.4, 0.44 sec (right). The transresonant nonlinear evolution of surface water waves accompanied by the strong change of the wave forms and by the eruption of the particles from wave tops. Similar waves may be in the scalar fields.

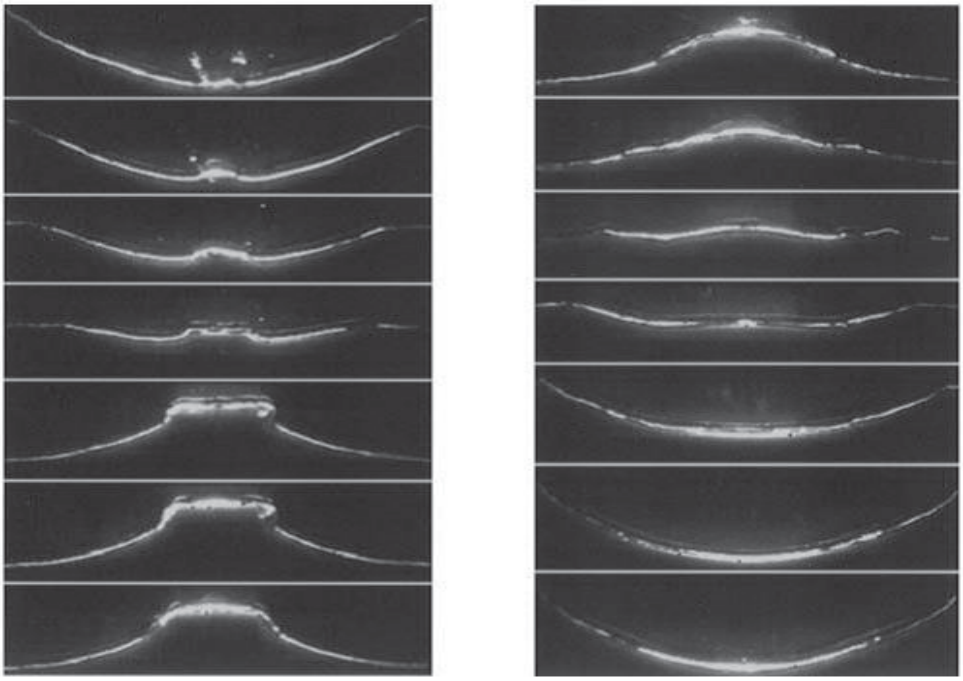

B. Gravity waves observed at the moments of time: 0.52, 0.56, 0.6, 0.64,0.68, 0.72, 0.76 (left), 0.8, 0.84, 0.88, 0.92, 0.96, 1, 1.04 sec (right). Similar waves may be in the scalar fields.

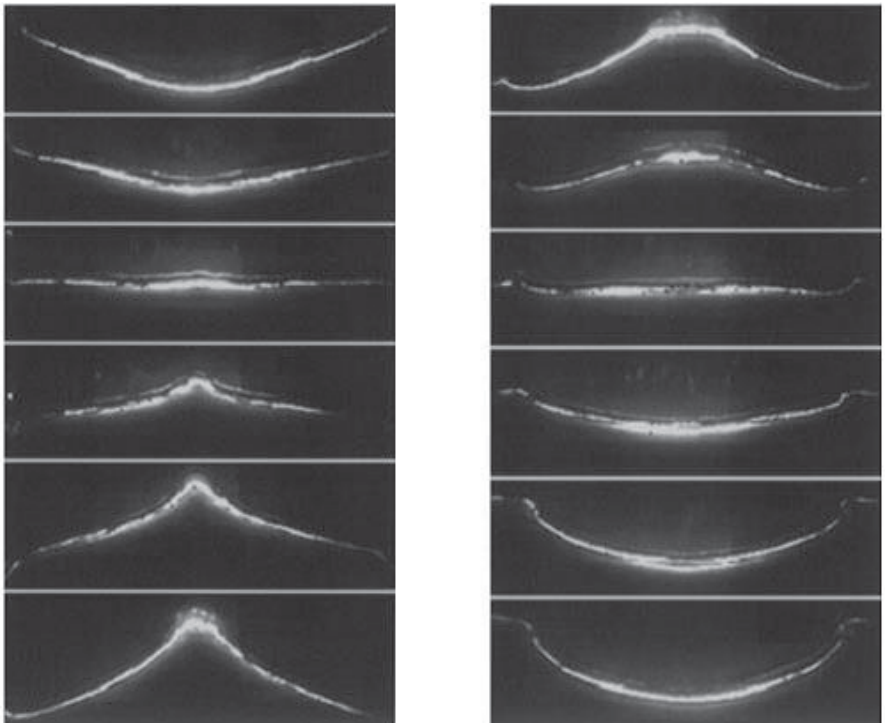

C. Gravity waves observed at the moments of time: 1.16, 1.2, 1.24, 1.28,1.32, 1.36 (left), 1.46, 1.5, 1.54, 1.58, 1.62, 1.66 sec (right). Similar waves may be in the scalar fields far enough from resonances.

Fig. 36. The transresonant nonlinear evolution of surface water waves accompanied by the strong change of the wave forms and by the eruption of the particles from wave tops (see A) [25].

Very wide spectra of strongly nonlinear waves are presented in Fig. 36. It is clear that waves of Fig. 36 are described qualitatively by our theory. In particular, Fig. 33 corresponds to Fig. 36A, Fig. 34 corresponds to Fig. 36B and Fig. 35 corresponds to Fig. 36C. However, there are some discrepancies between the observations and the calculations.

In our calculations we assumed that the shift of the linear oscillations (linear component of the solution) relative to the nonlinear oscillations (nonlinear component of the solution) was $-\pi/2$ (65). Generally speaking, this value is not known. The shift can be anything from 0 to $-\pi$. Certain discrepancies between the observations and the calculations can be explained by the variance in the value of the shift.

4.2. . Interface instability and Euler's spiral

Mechanisms of the origin of Faraday's strongly-nonlinear waves is not entirely clear. In particular, we do not know of examples of analytical modeling of them except our researches [16-19, 29, 35]. According to them, certain Faraday's waves are the sum of the elastica-like waves and linear harmonic waves.

We will not dwell here on the method of calculating the elastic-like waves. We only note that it is reduced to the solution of the algebraic equation (59). Then some travelling harmonic wave is added to the solution. The essence of the settlement compared their results with experimental data.

1. Fig. 37 shows the sum of harmonic wave and elastica-like wave passing some resonant band. This figure is taken from [19]. Fig. 37 qualitatibely describes experimental data shown in Fig. 38 and 39.

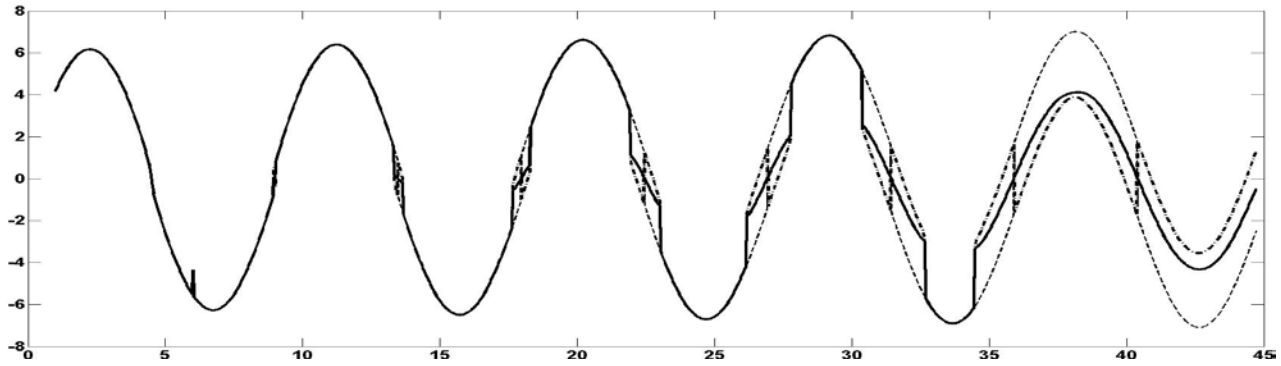

Fig. 37. Unidirectional waves crossing the resonant band. A process of an appearance of strongly nonlinear waves and folds of the wave profile .

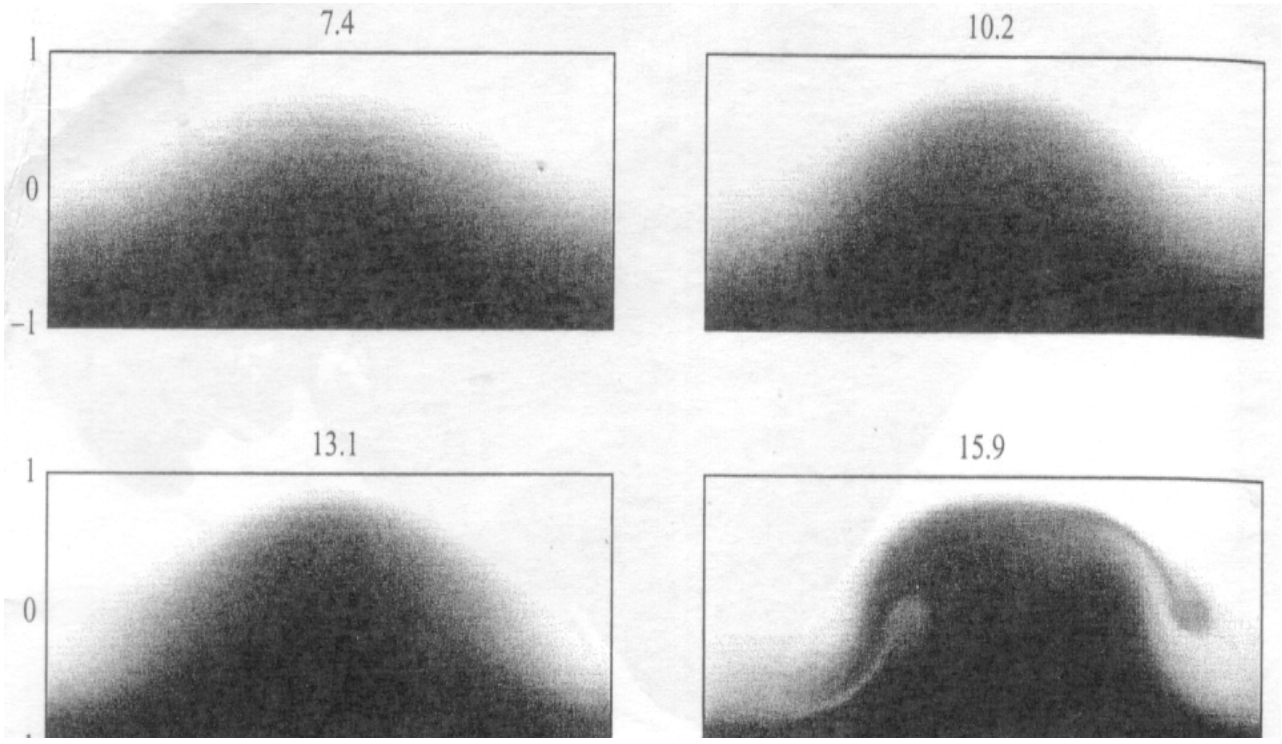

Fig. 38. Wave evolution of an interface of two liquids [47].

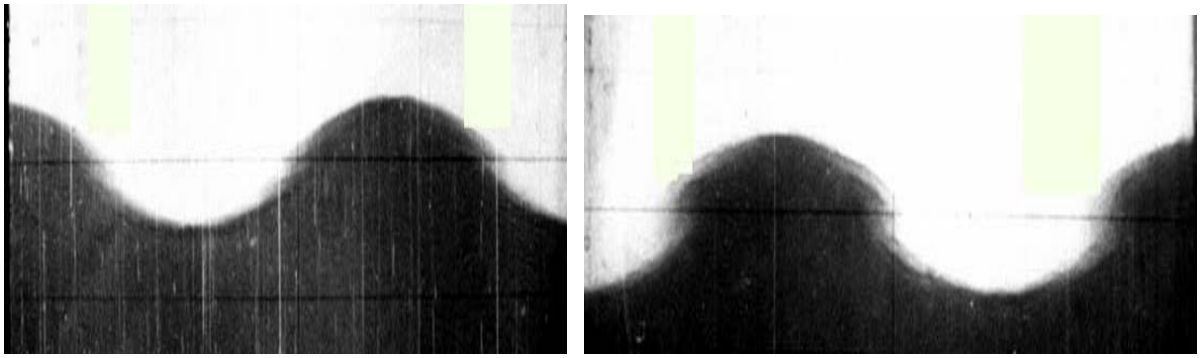

Fig. 39. Wave evolution of an interface of two liquids [28].

2. The Euler spiral can be considered something of a cousin to the elastic [48]. In particular, this spiral partly coincide with so-called the rectangular elastica (the case $\lambda \approx 0.5$ in Fig. 2). A sum the spiral and the rectangular elastica resembles the breaking wave (Fig. 40 left). It is interested that this sum may be qualitatively simulated by the sum of harmonic wave and elastic-like wave passing some resonant band (Fig. 40 centre and right).

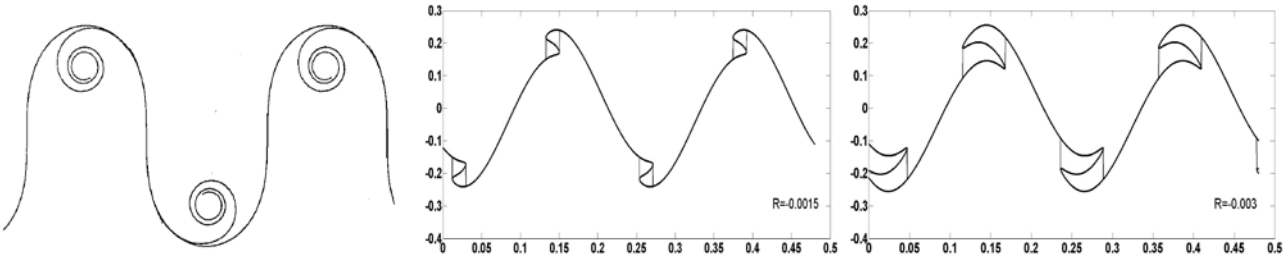

Fig. 40. A sum the spiral and the rectangular elastica (left). The sum of harmonic wave and elastic-like wave passing some resonant band (centre and right).

Thus, we have shown in the sections 3 and 4 that some elastica forms may describe not only the travelling wave. They can describe complex wave phenomena in different resonators. In particular, an appearance of surface cavities (bubbles), craters and jets may be described of the theory. Probably, something similar can occur with very strong seaquakes and earthquakes. The eruption of liquid from wave crests (Figs. 31-33) strikingly resembles volcano eruptions. On the other hand, these figures can illustrate the radiation of particles of mass and energy during the eruption of the Universe from the pre-unverse.

5. Conclusion

In the research we tried to consider many strongly–nonlinear phenomena based mainly on the classical Euler's results. We presented the scheme of the theory describing strongly nonlinear waves both in continuum and scalar fields. The theory describes the wide spectrum of the wave phenomena which have a resonant nature. The theory describes many elastica forms, which attracted the attention of many of the brightest minds in the history of mathematics and physics, including Galileo Galilei, James Bernoulli, Leonhard Euler, Pierre Laplace, Michael Faraday, Gustav Kirchhoff , Max Born and others [1-4, 15, 16]. We have shown the similarities of nonlinear phenomena which take place from oscillations of water surface through to the origin of the Universe.

Our purpose is to emphasize the common character of results presented in [16-19, 29, 35]. We have shown that there are similarities of highly-nonlinear wave phenomena in many areas of wave dynamics. We think that up to now highly-nonlinear wave phenomena have been poorly understood. Is there a universal, generic theory that can describe all these wave phenomena? We believe that such a theory may be created for 1-dimensional waves which are sufficiently long [16-19, 29, 35]. We also believe that similar theory, when applied to the nonlinear Klein-Gordon equation might shed light on the emergence and initial evolution of the Universe.

Acknowledgments

We thank Professor Brian Mace (the University of Auckland) for the support of this research. We had useful discussions of our results with him, Professor Garry Tee (the University of Auckland) and Professor Nail Akhmediev (Australian National University) .

References

[1] R. Levien, The elastica: a mathematical theory, http://levien.com/phd/elastica_hist.pdf .

[2] A. E. H. Love, A Treatise on the Mathematical Theory of Elasticity, Dover Publications, fourth edition (1944).

[3] C. Truesdell, Der Briefwechsel von Jacob Bernoulli, chapter Mechanics, especially Elasticity, in the Correspondence of Jacob Bernoulli with Leibniz, Birkhäuser (1987); C. G. Fraser, Mathematical Technique and Physical Conception in Euler's Investigation of the Elastica, Centaurus **34** (3), 211 (2007).

[4] V.G.A. Goss, Snap buckling, writhing and loop formation in twisted rods. Thesis of Doctor of Philosophy. The University of Lndon, 2003.

[5] J.J. Bernoulli, Quadratura curvae, e cujus evolutione describitur inflexae laminae curvatura, Die Werke von Jakob Bernoulli: Bd. 5: Differentialgeometrie, Birkhäuser, pp. 223–227, 1999 [1692. Med. CLXX; Ref. UB: L Ia 3, p. 211–212].

[6] L. Euler. Methodus inveniendi lineas curvas maximi minimive proprietate gaudentes, sive solutio problematis isoperimetrici lattissimo sensu accepti, chapter Additamentum 1. eulerarchive.org E065, 1744.

[7] P. S. Laplace. Œuvres complètes de Laplace, volume 4. Gauthier-Villars, 1880. Volume 4 of Laplace's Complete Works [19, pp. 349–401].

[8] G. R. Kirchhoff, On the equilibrium and the movements of an infinitely thin bar, Crelles J. Math. 56 (1859).

[9] M. Born, Untersuchungen über die Stabilität der elastischen Linie in Ebene und Raum, unter verschiedenen Grenzbedingungen. PhD thesis, University of Göttingen (1906).

[10] M. Born. My Life and Views, Scribner (1968).

[11] N.Jones, Structural Impact, Cambridge University Press, Cambridge (1989).

[12] D.Raragiozova, N. Jones, On dynamical buckling phenomena in axially loaded elastic-plastic cylindrical shells, Int. J. Non-linear Mech. **37**, 1223 (2002).

[13] A.Pocheau, B. Roman, Uniqueness of solutions for constrained Elastica, Physica D **192**, 161 (2004).

[14] G.I. Taylor, Instability of jets, threads, and sheets of viscous fluid, In: Proceedings of the 12th Inter. Cong. of Applied Mech., Stanford (1968), Springer-Verlag, Berlin (1969).

[15] M.Faraday, On a peculiar class of acoustical figures and on certain forms assumed by groups of particles upon vibrating elastic surface, Phil. Trans. R. Soc. Lond. **52**, 299 (1831).

[16] Sh. U. Galiev, Topographic effect in a Faraday experiment, J. Phys. A: Math. Gen. **32**, 6963 (1999).

[17] Sh. U. Galiev, T. Sh. Galiyev, Eruption of the Universe out of a pre-universe. http://hdl.handle.net/2292/30899 .

[18] Sh. U. Galiev, Геофизические Сообщения Чарльза Дарвина как Модели Теории Катастрофических Волн (Charles Darwin's Geophysical Reports as Models of the Theory of Catastrophic Waves), Centre of Modern Education, Moscow (in Russian) (2011).

[19] Sh. U. Galiev, Darwin, Geodynamics and Extreme Waves, Springer (2015).

[20] B. Marts, A. Hagberg, E. Meron, A.L. Lin, Bloch-front turbulence in a periodically forced Belousov-Zhabotinsky reaction, Phys. Rev. Lett. **93**, 108305 (2004).

[21] I.A.Waitz, E.M. Greitzer, C.S.Tam, Aero–propulsion systems, in Fluid Vortices. Ed. Green, S.L. Kluwer Academic Publishers, 1995.

[22] C.E. Niederhaus, J.W. Jacobs, Experimental study of the Richtmyer-Meshkov instability of incompressible fluids, J. Fluid Mech. **485**, 243 (2003).

[23] A.J. James, B.Vukasinovich, M.K. Smith, A. Glezer, Vibration-induced drop atomization and bursting, J. Fluid Mech. **476**, 1 (2003).

[24] Sh. U. Galiev, The theory of non-linear transresonant wave phenomena and an examination of Charles Darwin's earthquake reports, Geophys. J. Inter. **154**, 300 (2003).

[25] L. Jiang, M. Perlin, W.W. Schultz, Period tripling and energy dissipation of breaking standing waves, J. Fluid Mech. **369**, 273 (1998).

[26] S.A.Thorpe, On standing internal gravity waves of finite amplitude, J. Fluid Mech. **32**, 489 (1968).

[27] V.A. Kalinichenko, Nonlinear effects in surface and internal waves of Faraday, Dissertation, Russian Academy of Sciences, Ishlinsky Institute for Problems in Mechanics (2009) (in Russian).

[28] V.A. Kalinichenko, Nonlinear effects in surface and internal waves of Faraday. Dissertation, Russian Academy of Sciences, Ishlinsky Institute for Problems in Mechanics, pp. 212 (2010) (in Russian).

[29] Sh. U. Galiev, T. Sh. Galiyev, Nonlinear transresonant waves, vortices and patterns: From microresonators to the early Universe, Chaos **11**, 686 (2001).

[30] А.Т. Филиппов, Многоликий солитон. М., Наука, 1986 (in Russian) (A.T. Filippov, The Versatile Soliton, Birkh*ä*user, Boston (2010)).

[31] V. A. Vakhnenko, Solitons in a nonlinear model medium, Phys. A: Math. Gen. **25**, 4181 (1992).

[32] A. Sakovich, S. Sakovich, Slitary wave solutions of the short pulse equation. J. Phys. A: Math. Gen. 39, L361 (2006).

[33] E. J. Parkes, Some periodical and solitary travelling-wave solutions of the short pulse equation, Chaos, Solitons and Fractals **38**, 154 (2008).

[34] Sh. U. Galiev, Transresonant evolution of wave singularities and vortices, Phys. Lett. A **311**, 192 (2003).

[35] Sh. U. Galiev, T. Sh. Galiyev, Scalar field as a model describing the birth of the Universe, InterNet. Galiev – Galiyev 18–12–2013 (2013); Sh. U. Galiev, T. Sh. Galiyev, Nonlinear scalar field as a model describing the birth of the Universe, Известия Уфимского Научного Центра Российской Академии Наук (Herald of Ufa Scientific Center, Russian Academy of Sciences (RAS)) **2**, 7 (2014); Sh. U. Galiev, T. Sh. Galiyev, Coherent model of the births of the Universe, the dark matter and the dark energy. https://researchspace.auckland.ac.nz/handle/2292/23783 (2014).

[36] M. Remoissenet, Waves Called Solitons, Springer-Verlag (1996); L.A. Ostrovsky, A.I. Potapov, Modulated Waves. Theory and Applications. The Johns Hopkins. Univ. Press, Baltimore and London (1999).

[36a] R. Grimshaw, A. Slunyaev, E. Perinovsky, Generation of solitons and breathers in the extended Korteweg-de Vries equation with positive cubic nonlinearity, Chaos **20**, 013102 (2010).

[37] E.Farhi, N.Graham, A.H. Guth, N. Iqbal, R.R. Rosales, N. Stamatopoulos, Emergence of oscillons in an expanding background, Phys Rev D **77**, 085019 (2008).

[38] M.A. Amin, R. Easther, H. Finkel, R. Flauger, M.P. Hertzberg, Oscillons after inflation, Phys. Rev. Lett. **108**, 241302 (2012).

[39] A. Ijjas, P. J. Steinhardt, A. Loeb, Inflationary paradigm in trouble after Planck2013, Phys. Lett. B **723**, 261 (2013).

[40] A. Ijjas, P. J. Steinhardt, Implications of Planck2015 for inflationary, ekpyrotic and anamorphic bouncing cosmologies, Class. Quantum Grav. **33**, 044001 (2016); N. Afshordi, J. Magueijo, The critical geometry of a thermal big bang, Phys. Rev. D **94**, 101301 (2016); S. M. Carroll, In What Sense Is the Early Universe Fine-Tuned? arXiv:1406.3057v1 [astro-ph.CO].

[41] Planck Collaboration (P. A. R. Ade *et al.*), Planck intermediate results. XIX. An overview of the polarized thermal emission from Galactic dust, A&A **576**, A104 (2015).

[42] Sh. U. Galiev, T. Sh. Galiyev, Simple model of the origin of the Universe. Известия Уфимского Научного Центра Российской Академии Наук (Herald of Ufa Scientific Center, Russian Academy of Sciences (RAS)) **4**, 27 (2016).

[43] J. Mureika, D. Stojkovic, Detecting vanishing dimensions via primordial gravitational wave astronomy, Phys. Rev. Lett. **106**, 101101 (2011).

[44] D. Stojkovic, Vanishing dimensions: theory and phenomenology, arXiv:1304.6444 (hep-th).

[45] D. Stojkovic, Vanishing dimensions: a review, Mod. Phys. Lett. A **28** (37), 1330034 (2013).

[46] M. Brooks, Silence is olden, New Scientist **2973**, 34 (2014).

[47] O. Fringer, R.L. Street, The dynamics of breaking progressive interfacial waves, J. Fluid Mech. **494**, 319 (2003).

[48] R. Levien, The Euler spiral: a mathematical history, http://www.eecs.berkeley.edu/Pubs/TechRpts/2008/EECS-2008-111.html
[49] Sh. U. Galiev, T. Sh. Galiyev, Eruption of matter, dark energy and the Universe from a pre-universe, Internet (February 2017).